Helsinki University of Technology Laboratory of Biomedical Engineering
Department of Engineering Physics and Mathematics
Teknillinen korkeakoulu teknillisen fysiikan ja matematiikan osasto lääketieteellisen tekniikan laboratorio
Espoo 2004

THEORY, MODELLING AND APPLICATIONS OF ELECTROCARDIOGRAPHIC MAPPING

Kim Simelius

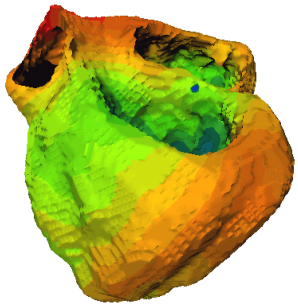

TEKNILLINEN KORKEAKOULU
TEKNISKA HÖGSKOLAN
HELSINKI UNIVERSITY OF TECHNOLOGY
TECHNISCHE UNIVERSITÄT HELSINKI
UNIVERSITE DE TECHNOLOGIE D'HELSINKI

Helsinki University of Technology Laboratory of Biomedical Engineering
Department of Engineering Physics and Mathematics
Teknillinen korkeakoulu teknillisen fysiikan ja matematiikan osasto lääketieteellisen tekniikan laboratorio
Espoo 2004

THEORY, MODELLING AND APPLICATIONS OF ELECTROCARDIOGRAPHIC MAPPING

Kim Simelius

Dissertation for the degree of Doctor of Technology to be presented with due permission for public examination and debate in Auditorium F1 at Helsinki University of Technology (Espoo, Finland) on November 10, 2004, at 12 o'clock noon.

Helsinki University of Technology
Department of Engineering Physics and Mathematics
Laboratory of Biomedical Engineering

Teknillinen korkeakoulu
Teknillisen fysiikan ja matematiikan osasto
Lääketieteellisen tekniikan laboratorio

ISBN 951-22-7027-7 (Printed version)
ISBN 951-22-7028-5 (Electronic version)
Tampereen Yliopistopaino Oy, Tampere 2004

HELSINKI UNIVERSITY OF TECHNOLOGY P.O. BOX 1000, FIN-02015 HUT http://www.hut.fi	ABSTRACT OF DOCTORAL DISSERTATION

Author Kim Simelius

Name of the dissertation

Theory, Modelling and Applications of Electrocardiographic Mapping

Date of manuscript April 3, 2004	Date of the dissertation
☐ Monograph	☑ Article dissertation (summary + original articles)

Department	Department of Engineering Physics and Mathematics
Laboratory	Laboratory of Biomedical Engineering
Field of research	Biomedical Engineering
Opponent(s)	
Supervisor	Toivo Katila, Prof., Helsinki University of Technology
(Instructor)	Jukka Nenonen, Doc., Helsinki University of Technology

Abstract

In this thesis, the genesis and applications of electromagnetic signals from the human heart are investigated through theory, modelling, signal processing and clinical studies.

One objective of the thesis was to develop and test signal processing methods that would be applicable to multichannel electro- and magnetocardiographic data. A signal processing method based on a type of neural networks called the self-organizing maps is introduced for spatiotemporal analysis of the body surface potential maps produced by the beating heart. This method is capable of utilizing both the spatial morphology of the potential distributions on the body surface as well as their temporal development. A signal processing method aimed at providing a reliable electric baseline for more traditional isointegral analysis of the body surface potential mapping (BSPM) data is also introduced.

Another objective of the thesis was to show the utility of electrocardiographic mapping in clinical use. This was demonstrated by applying electro- and magnetocardiographic mapping to evaluation of the propensity to life-threatening arrhythmias in postinfarction patients. Electrocardiographic mapping was found to perform equally well compared to more traditional SA-ECG, but electrocardiographic mapping may be more robust against individual variability in anatomy.

A third objective of the thesis was to build a computer model of the human heart that is capable of simulating the normal ventricular activation. The propagation model is based on a bidomain formulation of the cardiac tissue applied to realistic geometry of the ventricles. An anatomically accurate model of the human conduction system that reproduces measured activation sequence of the human heart was developed in this thesis. The body surface potentials and the magnetic fields computed from the simulated activation corresponded to recordings from normal subjects.

In summary, the thesis demonstrates the utility of electrocardiographic mapping in clinical use and introduces new signal processing methods that can be applied to this use. Finally, a computer model of the human heart binds together the physiology and anatomy of the human heart and body, classical electromagnetic theory, and computer science to explain the genesis and characteristics of the electromagnetic signals from the human heart.

Keywords Electrocardiography, BSPM, multichannel, heart model, bidomain, conduction system

UDC	Number of pages 158
ISBN (printed) 951-22-7027-7	ISBN (pdf) 951-22-7028-5
ISBN (others)	ISSN

Publisher

Print distribution

☑ The dissertation can be read at http://lib.hut.fi/Diss/ 2004/isbn9512270285

To Maija, Saana and Johannes

Miten mitata aikaa, petollista ja pakenevaa, joka aina liukuu käsistämme, niinkuin hieno hiekka heikosti sihisten vuotaa tiimalasista. Jokaiselle ihmiselle on aika erilainen, jokainen mittaa aikaa oman kehityksensä mukaan, ja aina pysähtyessään tuokioksi katsomaan taaksepäin ihminen näkee toimintansa ja tekojensa täydet vuodet pitkinä ja rikkaina takanaan, mutta tapauksettomat, vailla kehitystä kuluneet vuodet ovat kuluneet ohi jälkeä jättämättä silmänrävähdyksen lailla. Siten nuorelle miehelle pitkä matka uusine ihmisineen, vaihtelevine näkyineen ja kokemuksineen voi mahduttaa kuukauden sisään kehityksen, joka jälkeenpäin katsoessa vastaa kokonaisia vuosia. Vangille jokainen hetki on kuolettava ja pitkä kärsimättömyyden, toivon ja masennuksen vuoroin vaihdellessa, mutta jälkeenpäin hänen vankeusvuotensa ovat vierineet ohi tyhjinä ja sisällyksettä kuin kiitävin siivin. Ei elämällä sinänsä ole arvoa ihmiselle, vaan sillä, mitä meidän sallitaan elää.

Mika Waltari, Kaarina Maununtytär, *Luku 13*

Es destilliert aus Studien und Gedanken
Vielvieler Jahre spät ein alter Mann
Sein Alteswerk, in dessen krause Ranken
Er spielend manche süsse Weisheit spann.

Hinstürmt voll Glut ein eifriger Student,
Der sich in Büchereien und Archiven
Viel umgetan und den der Ehrgeiz brennt,
Ein Jugendwerk voll genialischer Tiefen.

Er sitzt und bläst ein Knabe in den Halm,
Er füllt mit Atem farbige Seifenblasen,
Und jede punkt und lobpreist wie ein Psalm,
All seine Seele gibt er hin im Blasen.

Und alle drei, Greis, Knabe und Student
Erschaffen aus dem Maya-Schaum der Welten
Zaubrische Träume, die an sich nichts gelten,
In welchen aber lächelnd sich erkennt
Das ewige Licht, und freudiger entbrennt.

Hermann Hesse, Das Glasperlenspiel, *Seifenblasen*

Contents

Preface and Acknowledgements

This thesis was written partly at the Laboratory of Biomedical Engineering at Helsinki University of Technology and at the Department of Physiology at Dalhousie University. My work for the thesis was supervised by professor Toivo Katila to whom I extend my gratitude for the continuing support, hands-on mentoring in classical field theory, and for providing the excellent facilities available to our research team. For the whole duration of my thesis work, I have received invaluable guidance from my tutors, Dr. Jukka Nenonen and professor Milan Horáček, and enjoyed making science at its best, as we spent long hours on the heart model in Halifax. Especially Jukka has offered his generous help and support to me ever since I was a young student. Moreover, it has been a pleasure and a challenge to work in a laboratory that has as close connections to the clinical world as ours does. Bridging this gap, I feel grateful to our fruitful research team consisting of M.Sc. Matti Stenroos, M.Sc. Tommi Jokiniemi, Dr. Lutz Reinhardt, M.Sc. Mats Lindholm, Dr. Juha Montonen, Dr. Jyrki Lötjönen, M.Sc. Mika Paavola, Dr. Panu Takala, Dr. Katja Pesola, M.Sc. Heikki Väänänen, M.Sc. Antti Pursula, Mr. Ville Mäntynen, MD Ilkka Tierala, Dr. Helena Hänninen, Dr. Petri Korhonen, Dr. Markku Mäkijärvi and Dr. Lauri Toivonen. The international connections to Germany, the Netherlands and to Canada have brought me the pleasure to work and get support from various people, of whom I would specially like to mention Dipl.-Phys. Hans-Jürgen Bruns, Dr. Thomas Fetsch, Dr. Coen Metting van Rijn, Dr. Cindy Penney, MD Petr Stovicek, Dr. Clyde Clements, Mr. Brian Hoyt and Mr. Paul McInnis. I also want to thank my current employer, Nokia, for the positive attitude towards this work and my studies, and especially M.Sc. Mika Lehtinen for supporting me in finishing the thesis.

The people I have mentioned above are those who contributed to my work in some manner, and as unfortunate as it is, I may have left people out from this list either intentionally or by accident. However, my work for this thesis would have been significantly more difficult had I not had those many friends like Kimmo, Mika, Petri and Jyrki with whom I spent many enjoyable moments relaxing and enjoying life.

This research work was supported by Vilho, Yrjö and Kalle Väisälä Foundation, Magnus Ehrnrooth Foundation, Emil Aaltonen Foundation, Instrumentarium Science Foundation, Aarne Koskelo Foundation, Jenny and Antti Wihuri Foundation, the Cultural Foundation of Pirkanmaa, and Nokia Corporation. I thank these institutions sincerely for their material support.

I wish to thank Docent Timo Mäkikallio and Professor Jari Hyttinen for examining the thesis and providing guidance to improving it. Their remarks and suggestions will also be valuable in continuing the work.

This work is all about the human heart, wherever we believe that is located in relation to the thorax. Although my work and duties sometimes bring me to faraway places or make me stay at work, my heart is always at home with my loving wife Maija, our beautiful and peppery daughter Saana and our smiling son Johannes. It took a long time for Maija, Saana and eventually Johannes to follow my dream come true, and it has been a huge sacrifice, and from now on I want to do my best to make their dreams come true, whatever they may be or become. During the time of the work I have noticed that I also carry with me the hearts of other people in my large family like my mother and father and two dear brothers Jani and Juha, and I wish I am sometimes able to make their hearts a little bit lighter.

Tampere, September 6, 2004

Kim Simelius

List of publications

This thesis consists of an overview and of the following six publications:

I K. Simelius, M. Stenroos, L. Reinhardt, J. Nenonen, I. Tierala, M. Mäkijärvi, L. Toivonen and T. Katila. Spatiotemporal characterization of paced cardiac activation with body surface potential mapping and self-organizing maps. *Physiol. Meas.* **24**, 805–816, 2003.

II T. Jokiniemi, K. Simelius, J. Nenonen, I. Tierala, L. Toivonen and T. Katila. Baseline reconstruction for localization of rapid ventricular tachycardia from body surface potential maps. *Physiol. Meas.* **24**, pp. 641–651, 2003.

III H. Väänänen, P. Korhonen, J. Montonen, M. Mäkijärvi, J. Nenonen, L. Oikarinen, K. Simelius, L. Toivonen and T. Katila. Non-invasive arrhythmia risk evaluation in clinical environment. *Herzschrittmachertherapie & Elektrophysiologie* **11**, 229–234, 2000.

IV P. Korhonen, I. Tierala, K. Simelius, H. Väänänen, M. Mäkijärvi, J. Nenonen, T. Katila and L. Toivonen. Late QRS activity in signal-averaged magnetocardiography, body surface potential mapping, and orthogonal ECG in postinfarction ventricular tachycardia patients. *Ann. Noninvasive Electrocardiol.* **7**, 389–398, 2002.

V K. Simelius, J. Nenonen, V. Mäntynen, J.C. Clements and B.M. Horáček. A Hybrid Model of Cardiac Electrical Conduction. *Helsinki University of Technology Report TKK-F-A829*, 2004.

VI K. Simelius, J. Nenonen and B.M. Horáček. Modeling cardiac ventricular activation. *International J. on Bioelectromagnetism* **3**, pp. 51–58, 2001.

List of symbols

v_m	Membrane potential (mV).
j_m, i_m	Membrane current (A/cm^2).
$\vec{p}$	Current dipole (Am).
j^i	Impressed current density (A/cm^2).
j_p	Primary current density (A/cm^2).
j_{ohm}	Ohmic (passive) current density (A/cm^2).
j_i	Intracellular current density (A/cm^2).
j_e	Extracellular current density (A/cm^2).
ϕ	Electric potential (mV).
$\vec{E}$	Electric field (V/m).
$\vec{B}$	Magnetic field (pT).
σ, σ_i, σ_e	Conductivity, intracellular and extracellular conductivity (mS/cm).
D_i, D_e	Intracellular and extracellular diffusion tensor, elements are conductivities (mS/cm).
C_m	Membrane capacitance per unit area ($\mu\mathrm{F}/\mathrm{cm}^2$).
χ	Surface-to-volume ratio for the myocardial cells (1/cm).
k	Ratio of intracellular and extracellular diffusion tensors for equal anisotropy ratios (unitless).
I_s	Current per unit area (A/cm^2).
τ	Current dipole strength per unit area (A/cm).
ϕ_∞	Electric potential caused by a source in an infinite homogeneous conducting media (mV).
$\vec{B}_\infty$	Magnetic field caused by a source in an infinite homogeneous conducting media (pT).

1 Introduction

The electrocardiogram has been used to study the heart noninvasively for one hundred years since the first recording by Einthoven in the year 1902. A standardized way of measuring and interpreting the electrocardiogram was proposed already in 1913 by Einthoven [29]. Since that, the electrocardiogram has been one of the most used clinical analysis tools among auscultation by the stethoscope and measurement of blood pressure by the blood pressure gauge. These three examination methods provide simple ways to study the heart from three different angles: the mechanical function, the cardiac output and pressure generation, and the electrical function.

The disciplines of electro- and magnetocardiography aim at the recording and analysis of the cardiac electromagnetic signals generated by the beating heart [139, 5]. By measuring such electromagnetic signals it is possible to diagnose and characterize several life-threatening diseases of the heart, like arrhythmias, ischemia, infarction and hypertrophy, amongst others. These techniques are completely noninvasive, and thus they are valuable tools in planning and guiding of the diagnosis and treatment of cardiac patients.

During the past few decades, the technologies in the field of bioelectricity and biomagnetism have evolved significantly. The long-term trend in this development has been towards multichannel measurement devices and effective analysis software for clinical use [38]. A contemporary electrocardiographic mapping system may feature more than one hundred channels each having characteristics similar to a high-resolution ECG system [90]. Multichannel magnetocardiographic mapping in clinical environment, covering the whole frontal chest has also become possible in recent years [86].

In this thesis, it is claimed that (1) advanced signal processing methods need to be developed to be able to properly analyze and to take full advantage of the multichannel body surface potential mapping data and magnetocardiographic data; (2) with advanced signal processing methods, body surface potential mapping is a viable clinical tool; (3) body surface potential mapping can be used to validate the propagation models of the heart and the anatomical models of the thorax; and (4) realistic models of the human heart together with comprehensive body surface potential mapping data are useful in non-invasive cardiac research. Proving these claims has provided the motivation for the individual works in this thesis.

Since the thesis covers a range of subtopics from clinical studies and practical work to computer modelling and electromagnetic theory, the layout of the thesis deviates from the traditional one. It was considered most appropriate to present the details of physiology, physics and engineering employed in this thesis to serve as a basis for understanding the modelling work. For this reason, the results of each sub-topic have been presented in the context of the materials and methods for the same sub-topic. In chapter 2, the anatomy, histology and electrophysiology of the human heart are described. The sources that create the cardiac electromagnetic signals are then introduced and analysed theoretically in chapter 3. The recording and analysis methods for the electromagnetic signals, as well as the patient studies carried out in this work, are described in chapter 4. Modelling of the human heart and the simulation results are presented in chapter 5. In the last chapter, the methods and results of this work are discussed in a summarizing manner.

Publications I and II present some novel signal processing methods that are suitable for the analysis of body surface potential mapping data. Publication I introduces a novel method based on self-organizing maps for analyzing the spatiotemporal behaviour of body surface potential maps. Publication II shows how the zero potential level during a fast ventricular tachycardia can be found automatically. Publications III and IV present the application of body surface potential mapping to clinical studies. Publication III extends the traditional signal averaging criteria and presents the use of signal-averaged body surface potential mapping data. Publication IV compares the performance of body surface potential mapping, magnetocardiographic mapping and signal-averaged orthogonal three-lead electrocardiograms. Publications V and VI present the use of a realistic heart model to model normal activation of the human heart. Publication V introduces new computational methods for the heart model, and Publication VI describes the propagation modelling and computations of extracardiac fields in the normal heart.

2 The Heart

2.1 Anatomy of the heart

The heart has four chambers, two atria and two ventricles, through which the blood is pumped (Fig 1). Valves control the direction of the blood flow. The wall of the heart includes a fibrous "skeleton" for attachment of the valves, the cardiac muscle, and a specialized conduction system.

The cardiac cycle starts with the contraction of the atria, with subsequent blood flow from the atria to the ventricles. As the ventricles are contracting during the systolic phase, blood is pumped from the left ventricle to the systemic circulation, and from the right ventricle to the lungs. During the diastolic phase, the atria and also to some extent the ventricles are again filled with blood. The atrial walls are thinner than the ventricular walls, accounting to the pressure generation function of the ventricles. Normally, the wall thickness of the right ventricle is about 0.5 cm and on the left ventricle about 1.5 cm. However, the volume of fully expanded ventricles is approximately the same.

The ventricular conduction system of the heart was observed by Purkinje already in 1845 on the endocardial surface of the sheep [108]. After the discovery of the atrioventricular node and the His bundle at the end of the last century [33, 48], Tawara presented his famous works on the conduction system of the heart [134]. He suggested that the so far mysterious Purkinje network was in fact a continuation of the His bundle, and that the conduction of the electrical signal took place along this network at a faster rate than through the rest of the myocardium. Tawara presented the conduction network for five species, including the man, and also studied the intraspecies differences in subjects of different ages. Later investigations confirmed the apparent differences between species that Tawara showed [136, 88]. The interindividual variability in man has also been shown to be significant [23, 25], not only depending on the age of the subject.

The anatomy of the human cardiac conduction system is complex [88] and the interindividual variability is large [23, 25]. However, this complexity in the conduction network exists mainly to provide necessary redundancy to this critical system. Therefore, it is possible to derive from anatomical and histological studies the features that a normal conduction system must possess.

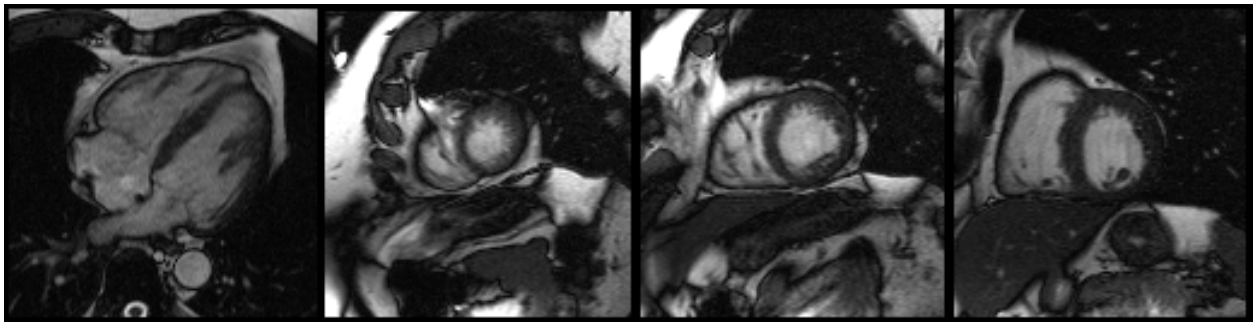

Figure 1: *Four cross sections of the heart from left to right: a slice along the long axis of the heart showing the four chambers and the papillary muscles, and three slices from the apex towards the base corresponding to layers 50, 70 and 90 in Fig. 21.*

The ventricular conduction system starts from the atrioventricular node (node of Tawara) as the His bundle [48]. The His bundle passes through the atrioventricular ring (the penetrating bundle) into the membraneous interventricular septum. Usually, the bundle then travels for about 15 mm on the left side of the septum [88], and gives off the left and right bundle branches.

Although the structure of the conduction system in the left ventricle is generally described as bifascicular [109], this has no basis in the actual anatomy. The term “hemiblock" refers to functional anomalies of the left conduction system, but it is also electrophysiologically a very crude classification [24]. In anatomical studies, the left bundle branch has been found to be a sheet-like structure that covers a large portion of the interventricular septum [25]. The fascicles in the branch are highly interconnected. The anterior rim of the left bundle travels towards the left anterior papillary muscle, while the posterior rim is oriented toward the left posterior papillary muscle.

The right bundle branch usually begins from the most distal part of the His bundle [135]. It courses subendocardially and intramyocardially towards the right anterior papillary muscle. At the papillary muscle, it divides into fascicles that continue as the right Purkinje network leading the activation to the posterior papillary muscle and the right ventricular free wall.

In the human heart, the Purkinje fibers travel on the endocardial surface of the trabecular muscles. Although Tawara claims that even the distal Purkinje fibers can be seen as such, the anatomical investigations have usually required staining [88]. The Purkinje fibers are clearly visible in ungulates, and these animals have frequently been used in the studies of the conduction system [108]. One must, however, be careful in generalizing any anatomical details from one species, as it has been shown that the Purkinje network varies greatly between different species [134, 136]. For example, in the human heart no connection has been shown to exist between the endocardial Purkinje fibers and the midmyocardial (M) cells, although these cells resemble each other in their electrophysiological properties [147]. In contrast, the Purkinje fibers run also intramurally in the pig heart [136].

2.2 Cardiac histology

Muscle fibres contain a large number of myofibrils, which in turn are comprised of myofilaments (actin and myosin). The organization of the filaments gives the muscle’s characteristic cross-striations. The myofibrils are divided by Z discs crossing the fibril to sarcomeres that are the functional units of a muscle. The contraction of a muscle happens as the two types of myofilaments slide past each other. The energy for the contraction is provided by adenosine triphosphate (ATP). The movement of the fibrils is initiated by the presence of calcium that has been delivered by the sarcoplasmic reticulum of the myofibril.

The cardiac muscle fibres consist of several muscle cells aligned end to end and connected by so called intercalated discs that convey the electrical activation between cells. The electrical connection between two cells takes place through the gap junctions present in the intercalated discs. Some cells in the fibre may also join with two other cells creating a branching of the fibre (see Fig. 2). The cardiac muscle cells are usually approximately 100 μm long, and 10-40 μm in diameter. The shape and size of the cardiac muscle cells depends on their location in the heart, e.g., the cells on the epicardium or on the endocardium are typically smaller in diameter than intramural cells.

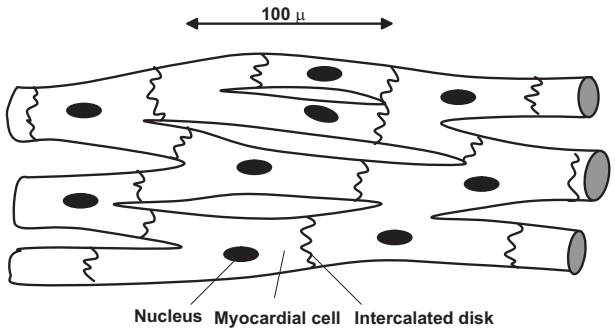

Figure 2: *Organization of the cardiac muscle. Long, cross-striated muscle fibres make up the cardiac muscle. Between cells, the electrical activation is conveyed by the intercalated discs. Branching is also typical of the cardiac muscle cells. Adapted from [110].*

The conduction system of the heart consists of specialized cardiac muscle cells. They convey the electrical impulse at a rate approximately four times faster (1–2 m/s) than the cardiac muscle cells (0.3–0.8 m/s) [22, 60]. The conduction system cells are responsible for the coordination of the contraction of the atria and ventricles, as they are the only active cells present within the heart's fibrous skeleton.

The cells in the conduction system are smaller than myocardial cells, and there are less transverse gap junctions between the cells [138, 87], which leads to higher conduction velocity in these cells. From the Purkinje network, the activation is conveyed to the myocardium by transitional cells in Purkinje-myocardial junctions (PMJs) [136]. The transitional cells amplify the current from Purkinje cells so that the low-impedance load of the myocardium does not hamper propagation in the conduction network [89]. This property may facilitate re-entry through the Purkinje system, as reported in some studies [10].

2.3 Metabolism in the heart

Cardiac muscle cells need energy primarily for two purposes: to carry out mechanical work (contraction and relaxation) and to maintain excitability with the aid of ion pumps. Like in any muscle, the cardiac muscle cells receive their energy from the breaking of the ATP molecules. These molecules are constructed again in the cell if sufficient oxygen is present. The oxygenation of the cardiac muscle cells is provided by coronary arteries and the cardiac microcirculation.

The coronary arterial circulation consists of arteries on the epicardium and in the cardiac muscle. Three major coronary arteries supply the heart: left anterior descending artery (LAD), left circumflex artery (LCX), and right coronary artery (RCA). Although all parts of the heart are supplied mainly by one coronary artery, in a normal heart there are several collateral arteries taking care of blood supply, e.g., in case of a narrowing in one coronary artery in coronary artery disease (CAD). However, these collateral arteries supply blood to subendocardial areas less than the coronary arteries.[110]

Decrease in blood supply to the cardiac muscle results in a development of ischemia or ultimately myocardial infarction, decreased availability of nutrition and buildup of metabolites. This syndrome is a result of, e.g., ischemic heart disease. The lack of blood supply causes "chest pain", i.e. angina pectoris, or in a more severe case a "heart attack", i.e. myocardial infarction. [68]

2.4 Membrane physics

Two processes control the transfer of active ions through membranes. The concentration gradient causes a diffusion flux according to Fick's first law (in one dimension)

$$J_i = -D_i \frac{dc_i}{dx}, \tag{1}$$

where J_i is the diffusion flux of ion i, D_i is the diffusion coefficient, and dc_i/dx is the concentration gradient of the ion. The flux due to electric potential difference is given by

$$J_i = -c_i \frac{z_i F}{RT} D_i \frac{dV}{dx}, \tag{2}$$

where z_i is the valence, F is Faraday constant, T the temperature and R the gas constant. When the ionic flows across the membrane due to the concentration gradient and the potential gradient are balanced, the membrane has reached the equilibrium potential of that ion given by the Nernst equation [47]

$$V_m = \frac{RT}{z_i F} \ln \frac{c_i^o}{c_i^i}, \tag{3}$$

where the supersripts refer to concentrations inside and outside of the membrane. If several ions are involved in the process, as is the case in the membranes of living cells, the potential is given by the Goldman-Hogdkin-Katz equation [37, 49]

$$V_m = \frac{RT}{F} \ln \frac{\sum_p P_p c_p^o + \sum_n P_n c_n^i}{\sum_p P_p c_p^i + \sum_n P_n c_n^o}, \tag{4}$$

where P_i is the permeability of the membrane for ion i and subscripts p refer to positive and subscripts n to negative ions.

In addition to diffusion and electrical leakage current, the transport processes of a living cell include active transport performed by ion pumps and ion channels. The ion pumps work to maintain preferred ionic concentrations inside the cell. The properties of these pumps and the active ion channels determine the membrane potential of the cell in static conditions, and govern the activation process of the cell membrane.

2.5 Action potential of the cardiac cell

The resting membrane potential of a cardiac muscle cell, defined against the potential of the extracellular medium, is between -80 mV and -95 mV, close to the Nernst potential of potassium. If this potential is raised above -60 mV due to activation from adjacent cells or leakage currents (pacemaker cells), an action potential is generated. First, the voltage sensitive sodium channels open letting sodium ions flow into the cell and depolarizing the membrane to +20 mV. In some cells, this rapid transition is followed by a plateau phase at 0 mV, when permeabilities for all ions are close to zero. The opening of the slower potassium channels starts the repolarization phase of the membrane, and the membrane potential returns to it's resting value, possibly through a modest undershoot. Small changes in the resting membrane potential are overcome by the increased potassium current due to deflection from the equilibrium potential of this ion.

After the fast upstroke of the membrane potential, the conductance of sodium decreases rapidly as the channels enter an inactive state due to depolarization of the membrane. The depolarization activates the influx of calcium ions, further leading to a massive release of calcium from the sarcoplasmic reticulum. The increase of intracellular calcium concentration starts the contraction of the muscle cell by acting on the troponin C in the myofilaments. At the same time, a transient outward current of potassium ions starts to repolarize the membrane. After the closing of calcium channels, the outward flux of potassium ions finishes the repolarization of the membrane, and the membrane potential returns close to the equilibrium potential of potassium. The ion pumps and many other smaller ionic currents also take part in the action potential of the cardiac muscle cell.[14]

Because of different forms of cells and different arrangements for action potential conduction between cells, different activation velocities appear in different tissue types. The typical conduction velocity in a long nerve ending is 10–100 m/s, whereas the velocity in a cardiac muscle cell is only about 0.3–0.8 m/s in longitudinal direction [22, 60]. The propagation speed depends also strongly on cardiac muscle fibre orientation: in the transverse direction, the propagation speed is less than half of the speed in longitudinal direction. In the cells belonging to the conduction system, the propagation velocity can be up to 2 m/s.

2.6 Electrical activation of the myocardium

During normal electrical activation, the pace of the rhythmic contractions of the heart is given by the sinotrial (SA) node. After the atria have activated, the impulse is picked up by the atrioventricular (AV) node and conducted to the endocardial surface of the ventricles by the bundle of His, the right and left bundle branches and the Purkinje fibres. Between the cardiac muscle cells, the electric excitation spreads through the gap junctions in the intercalated discs. The excitation finally spreads from the endocardium towards the epicardium, and the total volume of the cardiac muscle is normally activated within 100 ms.

The cardiac cycle begins with the spontaneous activation of the sinotrial node, followed by the activation of the right and left atria. The activation of the atria causes the P-wave of the ECG. Following the atria, the activation spreads slowly to the ventricles through the atrioventricular node (the AV node), allowing the atria to contract fully before the activation of the ventricles. After the AV node, the activation is conveyed rapidly to the ventricular muscle by a specialized conduction system consisting of the His bundle, the bundle branches and the network of Purkinje fibers. The ventricles are then activated essentially in the direction from endocardium to the epicardium, although some distinct intramural activation patterns are present due to the inhomogeneous distribution of the distal Purkinje network [28]. The activation of the ventricles causes the QRS-complex to appear on the ECG. The repolarization of the ventricles takes place more irregularly than the activation, since the action potential duration varies throughout the myocardium, and it results in the T-wave on the ECG. The repolarization of the atria is hidden underneath the QRS-complex.[44]

There are several disorders that can disturb the normal activation pattern of the cardiac muscle. The cause of atrial and ventricular tachyarrhythmias can be a group of cells displaying abnormal automaticity, or an area of slow conduction that has led to the development of a re-entrant circuit. The former type of arrhythmia is called focal arrhythmia, where the normal activation control of the

heart is taken over by this group of cells. The latter type is called re-entrant arrhythmia according to its origin. The re-entrant circuit causing these arrhythmias is an area of slow conduction with a unidirectional conduction block allowing the development of prolonged electrical activation in this area. When the activation exits to the normal cardiac muscle, a premature activation can be caused, and a series of these activations leads to a tachyarrhythmia.[1, 32, 70]

Atrial arrhythmias are typically caused by the development of a re-entrant circuit. The fractioned geometry of the atria supports the development of these circuits due to the many openings for the arteries and veins connecting to the heart. However, focal arrhythmias are also common.

Ischemia can cause the cardiac muscle cells to lose their ability to activate, and after myocardial infarction the damaged cells on the rim of the infarction display a highly altered activation pattern. The abnormal activation of these cells can lead to the development of areas of slow conduction and re-entry circuits. These areas are the cause for re-entrant tachyarrhythmias and also the development of more serious life-threatening conditions like spiral waves [61] or ventricular fibrillation. The areas of slow conduction frequently display continuous electrical activation. The risk for this type of ventricular arrhythmias can be recognized from the electromagnetic signals on the body surface by the high-frequency components present during or after the QRS complex. [39, 40]

Tachyarrhythmias can also be caused by abnormal conduction of the electrical activation between the atria and the ventricles. This type of arrhythmias include the so called Wolff-Parkinson-White (WPW) syndrome, where there is an accessory conduction pathway (AP) between an atrium and a ventricle. When the pathway conducts the electrical activation retrogradely, a re-entrant circuit consisting of the atrium, the AV node, the ventricle and the accessory pathway can be created. The accessory pathway can also conduct atrial fibrillation to the ventricles causing ventricular fibrillation. Another arrhythmia caused by abnormal conduction is AV nodal arrhythmia, where the AV pathway is divided in two and the other half is conducting retrogradely and presents a slower conduction velocity.[62]

2.7 Movement of the heart

The cardiac muscle is organized in a special manner to accommodate efficiently for the pumping task of the heart. The muscle fibres form layers of muscle that are not lined up with the long axis of the heart but mostly encircle the chambers as they go around the heart. These layers can also pass from the epicardium to the endocardium along their length [130, 66]. This special arrangement of the muscle fibers is responsible for the characteristic electrical anisotropy of the myocardium [57].

This special organization of the cardiac muscle causes a very characteristic movement during contraction, which can be seen with modern imaging facilities. For efficient pumping, the contraction starts from the inner parts of the cardiac muscle and spreads towards the epicardium. As the muscle contracts, the ventricular volume is diminished both by the twisting motion and the shortening of the muscle. This causes the heart to rotate and the base of the heart to move towards the apex during the muscle contraction.

3 Electrical sources in the heart

The electrocardiogram and magnetocardiogram are generated by the electrical activation of the cardiac muscle cells. Therefore, it is necessary to understand the origin of the cell membrane potential and the activation process of a single cell. When the cells activate in phase, they form larger entities that can best be modelled by surface sources or by multipole sources. The ECG and MCG result from the activation of these sources alternated and distorted by the inactive tissues of the body. Thus, the volume conductor properties of the thorax have to be modelled for calculating the electric and magnetic fields on the body surface, caused by the sources, i.e., for solving the forward problem in electro- and magnetocardiography [3, 51, 137]. The sources causing a measured electric potential or magnetic field pattern on the body surface can also be determined by solving the inverse problem of cardiography [52, 83, 38, 99].

3.1 Action potential models

Several models for the action potentials of different cells and the spreading of activation in the tissue have been proposed. For example, the Beeler-Reuter model of the cardiac action potential is based on the Goldman–Hodgkin–Katz (GHK) equations [6]. The GHK current equation describes the steady-state ionic currents of an excitable cell under simplifying assumptions of the membrane potential. One of the most comprehensive model for the ionic currents of an activating cardiac muscle cell has been presented by Luo and Rudy [81]. The model accounts for all known ionic currents of the cell by assigning a set of interdependent differential equations to the currents. Using this model, it is possible to reproduce accurately action potentials actually recorded from a cardiac muscle cell. To investigate the spatial behaviour of a propagating action potential, linear cable theory or realistic simulations can be used [95, 96].

3.2 Physiological sources and the electromagnetic fields

In the quasistatic approximation of the Maxwell equations, generally acceptable for the bioelectromagnetic phenomena [137], the source of the electric field is the electric charge and the source of the magnetic field is the electric current. When the cells in the cardiac tissue are at rest, the electric charge distribution creates a quickly vanishing field at distances large compared to the cell dimension, since there is no monopolar or dipolar distribution of charges present. At rest, there are no currents flowing either (in healthy tissue), and the magnetic field is also zero.

Macroscopically seen, the cardiac tissue can be considered a space, where every point is co-occupied by the intracellular space, the extracellular space and the cell membrane [35]. Each ionic charge is, however, occupying only either space at a time, and must move through the membrane to flow to the other space. Such formulation of the myocardium is called *the bidomain model*.

When there is a propagating wave front in the myocardium, the open ionic channels in the depolarized cells allow current to flow through the membrane. Due to the potential difference across the membrane, the depolarized cells act as current generators, and this current is decharging the capac-

itance of the neighbouring cells that have not depolarized yet. Since current must be solenoidal, the path of intracellular current, membrane current and extracellular current is completed by displacement current through the closed membrane (as we know, displacement current is not a real current). These currents extend about 1 mm into the neighbouring cells [145], which imposes some requirements on the modelling of the cardiac tissue; optimally, the cell size in the cardiac tissue models should be of the order of 100 μm. If a larger cell size is used, the effects of the larger simulation cell sizes have to be taken into account (see Publication V).

3.3 Models of sources

An electric charge creates a potential distribution and an electric field around it, and the electric field causes a current to flow according to

$$\vec{j}_{ohm} = \sigma\vec{E} = -\sigma\nabla\phi, \tag{5}$$

where $\vec{j}_{ohm}$ is the (Ohmic) current density, $\vec{E}$ the electric field and ϕ the electric potential. The above equation holds also for charge distributions, e.g., for the electric dipole. A current dipole is constructed from a current source and a current sink in a conducting medium. Such a dipole $\vec{p}$ is defined by

$$\vec{p} = I_o\vec{d}, \tag{6}$$

where I_o is the current flowing between the two charges and $\vec{d}$ is the dipole direction vector, usually defined as a metric vector from the current source location to the current sink location.

As pointed out above, bioelectromagnetic sources create two types of currents: the ohmic and thus conservative currents $\vec{j}_{ohm}$ according to Eq. 5 and impressed currents $\vec{J}^i$ due to the conversion of chemical energy to energy of the currents. It is also customary to define primary currents $\vec{J}_p$ as consisting of the impressed currents $\vec{J}^i$ and the ohmic currents driven by the impressed currents inside the cell (the intracellular current density $\vec{j}_i$) [137, 38, 99]. For example, the current in Eq. 6 can consist of the intracellular ohmic currents of a cardiac muscle cell. The total current flowing in the tissue is represented by

$$\vec{J} = -\sigma\nabla\phi + \vec{J}_p. \tag{7}$$

The total current includes also the ohmic currents flowing outside the source volume. According to continuity, $\nabla \cdot \vec{J} = 0$, and we get Poisson's equation in an infinite, homogeneous medium:

$$\nabla^2\phi = \frac{\nabla \cdot \vec{J}_p}{\sigma}. \tag{8}$$

The solution to this equation can be shown to be [103]

$$\phi(\vec{r}) = \frac{1}{4\pi\sigma}\int_{v'}\frac{-\nabla' \cdot \vec{J}_p}{|\vec{r} - \vec{r}'|}dv' = \frac{1}{4\pi\sigma}\int_{v'}\vec{J}_p \cdot \nabla'\left(\frac{1}{|\vec{r} - \vec{r}'|}\right)dv'. \tag{9}$$

If the conductivity of the medium is not homogeneous, the solution must be corrected to incorporate the effect of the changing conductivity. In the human body, the conductivities of cardiac and skeletal muscle, lungs, blood masses and other tissues differ significantly. Moreover, outside the body the conductivity is zero; the thorax surface causes the largest contribution to the solution. [137, 11]

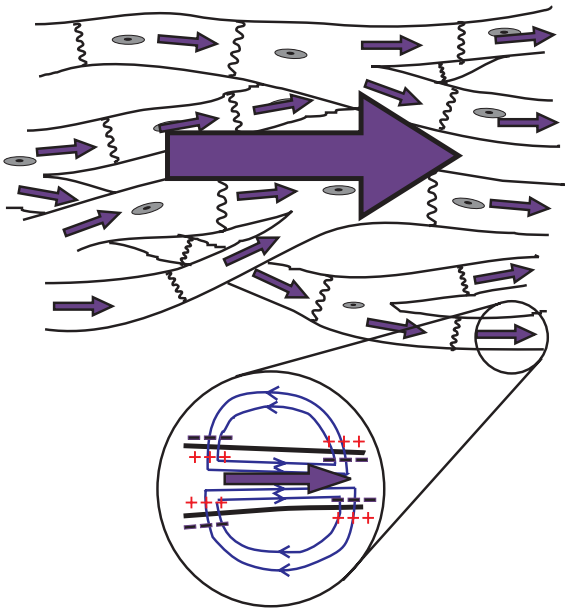

Figure 3: *The equivalent current dipole source. Microscopic current elements of individual cardiac muscle cells can be represented by a macroscopic dipolar source, provided that the cells are observed at a distance much larger than the cell dimensions. The activation is propagating to the right in this figure.*

The current dipole can be used as a source model for localization in cases where the the source volume is small, as is the case in focal arrhythmias. In Wolff-Parkinson-White syndrome, the pre-excitation due to the accessory pathway generates a dipolar field [100], as well as the exit sites of re-entry type ventricular arrhythmias. The three dipole moments (p_x,p_y,p_z) depend linearly on the field and are approximately proportional to the excited volume. Together with the (non-linear) spatial coordinates (x,y,z) the dipole is represented by six parameters.

In most cases, the total activation of the heart can be described with a surface source model. With a surface source we mean a construction where the extended equivalent source of electromagnetic field resides on a surface. In physiological conditions, the cellular activation can be modelled by

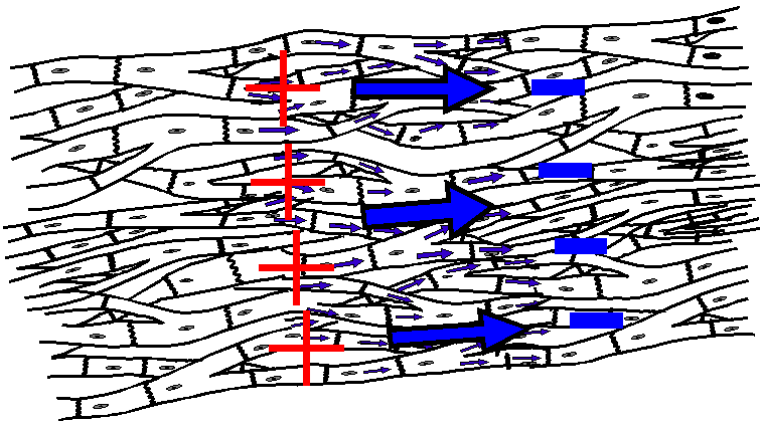

Figure 4: *Surface sources: the double layer. The activation wave front consists of numerous dipolar sources that form a double layer source. The signs plotted on the image represent the polarity of the intracellular potential.*

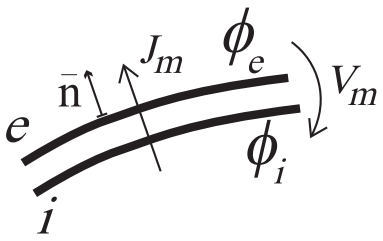

Figure 5: *Illustrations of membrane current J_m and potential $V_m = \phi_i - \phi_e$. The indices i and e refer to the intracellular and extracellular media, respectively.*

a simple charge or a dipole, and the corresponding surface sources are called the single layer and the double layer, respectively [52]. The double layers are usually created from activating cells, as shown in Fig. 4. Single layer sources arise as secondary sources on conductivity interfaces, when the volume currents induced by the primary current source accumulate charges on these interfaces. The cellular activity also creates both types of sources, as we will see in the following.

Let us define the single layer source as current $I_s(\vec{r}\,')$ per unit area, and the double layer source as current dipole strength $\vec{\tau}(\vec{r}\,')$ per unit area. The potentials arising from these sources are then

$$\phi^s(\vec{r}) = \frac{1}{4\pi\sigma} \int_{s'} \frac{I_s(\vec{r}\,')}{|\vec{r} - \vec{r}\,'|}\, dS' \tag{10}$$

for the single layer and

$$\phi^d(\vec{r}) = \frac{1}{4\pi\sigma} \int_{s'} \frac{(\vec{r} - \vec{r}\,') \cdot \vec{\tau}(\vec{r}\,')}{|\vec{r} - \vec{r}\,'|^3}\, dS' \tag{11}$$

for the double layer [103]. Analogically to the boundary conditions of the electrostatic field in matter, for the boundary conditions of an electric current field in a conducting medium we have

$$\phi_i - \phi_e = V_m \tag{12}$$

and

$$-\sigma_i \frac{\partial \phi_i(\vec{r}\,')}{\partial n} = -\sigma_e \frac{\partial \phi_e(\vec{r}\,')}{\partial n} = J_m(\vec{r}\,'), \tag{13}$$

where the indices i and e refer to media inside and outside the surface, respectively, V_m is the potential across the surface, i.e., $V_m = \phi_i - \phi_e$, and J_m is the current density through the surface in the direction of the surface normal (see Fig. 5). The notation above is adopted from the notation for sources in the cell membrane. The transmembrane potential and current can be related to the double layer and single layer sources, respectively, to obtain the electric potential created by the closed membrane of an active cell, or by any closed surface source:

$$\phi(\vec{r}) = \frac{1}{4\pi} \oint_{s'} \left(\frac{1}{\sigma_e} - \frac{1}{\sigma_i} \right) \frac{J_m(\vec{r}\,')}{|\vec{r} - \vec{r}\,'|}\, dS' + \frac{1}{4\pi} \oint_{s'} \frac{V_m(\vec{r}\,')}{|\vec{r} - \vec{r}\,'|^3} (\vec{r} - \vec{r}\,') \cdot d\vec{S}\,' \tag{14}$$

On macroscopic level, double layer sources are used, e.g., to represent the activation wave front in the cardiac muscle. Often, the double layer is assumed to be uniform in strength, for example to determine the activation timing by solving the inverse problem of electrocardiography [102]. It is then obvious from Eq. (14) that the potential generated by a closed uniform double layer vanishes. Furthermore, it can be shown that the electric potentials, created by two different double layer sources having an opening that covers the same solid angle observed from a field point, are identical. However, often it is necessary to use the oblique double layer as a source model, wherein the above simplifications are not possible.

From the previous it is clear that the potential distribution on the body surface created by the normal, activating heart can be approximated well by using a double layer as a source model. In this representation, the epicardial breakthrough of the cardiac activation is seen to play a special role. From Eq. 11 it can be deduced that the first large deflection in the potential on the body surface during normal activation is actually created by the opening of the double layer when the activation first reaches the epicardium of the right ventricle. Later, the nonuniform properties of the cardiac muscle play a more prominent role, and the intramural, non-uniform activation of the left ventricle also influences the body surface potential later in the course of normal activation.

3.4 Bidomain theory

In the bidomain theory for anisotropic myocardium, the intracellular and extracellular spaces co-occupy every point in the myocardium, and they are connected everywhere via the cell membrane [35]. A myocardial cell is approxomated as a long cylinder, so that the bidomain spaces have a dominant direction of fibers in every point — hence the term anisotropic myocardium. The fibre direction also sets the conductivity properties of the cell that govern the propagation (see Eq. 21). A more complete description of the anisotropic bidomain can be found in Ref.[35].

Let us denote the conductivity tensors in the intracellular and extracellular media as D_i and D_e, respectively [19]. According to Ohm's law, the current densities in the intracellular (i) and extracellular (e) space are

$$\vec{J}_{i,e} = -D_{i,e}\nabla\phi_{i,e}, \tag{15}$$

where $\phi_{i,e}$ are electrical potentials in these domains. Conservation of charge requires that the divergence of total current density vanishes under the quasi-static approximation [103], that is

$$\nabla \cdot \vec{J} = \nabla \cdot (\vec{J}_i + \vec{J}_e) = \nabla \cdot (D_i\nabla\phi_i + D_e\nabla\phi_e) = 0. \tag{16}$$

This implies that the transmembrane current is

$$i_m = \nabla \cdot D_i\nabla\phi_i = -\nabla \cdot D_e\nabla\phi_e, \tag{17}$$

since current can only flow from one domain to the other through the membrane. If we define a bulk conductivity tensor $D = D_i + D_e$, and notice, that the membrane potential $v_m = \phi_i - \phi_e$, we get from Eq.(16)

$$\nabla \cdot D\nabla\phi_e = -\nabla \cdot D_i\nabla v_m. \tag{18}$$

This is an elliptic partial differential equation describing the source of extracellular potential. The term $\nabla \cdot D_i\nabla v_m$ is the divergence of *impressed current density* $\vec{J^i} = -D_i\nabla v_m$[103].

The cable equation for transmembrane current states [60]

$$i_m = \chi\left(C_m\frac{\partial v_m}{\partial t} + I_{ion} - I_{app}\right), \tag{19}$$

where χ is the membrane surface area per unit volume of the tissue, C_m the membrane capacitance per unit area of the membrane surface, I_{ion} the ionic current per unit area of the membrane surface, and I_{app} any externally applied current. Using χ to express the above equation in terms of current densities, we get

$$c_m\frac{\partial v_m}{\partial t} - \nabla \cdot D_i\nabla v_m + i_{ion}(v_m) = \nabla \cdot D_i\nabla\phi_e + i_{app}, \tag{20}$$

which is a parabolic partial differential equation in v_m. We will further make the assumption that $D_e = kD_i$, i.e., we assume the ratios of transverse and axial conductivities to be the same in intracellular and extracellular space. Equations (18) and (20) can then be simplified to give a generalized cable equation [74]

$$c_m \frac{\partial v_m}{\partial t} = \nabla \cdot D_k \nabla v_m - i_{ion}(v_m) + i_{app}, \tag{21}$$

where $D_k = \frac{k}{1+k} D_i$. The generalized cable equation is computationally simpler to apply, and even under modest deviation from the assumption $D_e = kD_i$ may provide accurate results, if the conductivities are chosen properly. Equation (21) governs the subthreshold behaviour of the model elements. In a discrete model, the term $\nabla \cdot D_k \nabla v_m$ can be computed from

$$\begin{aligned} \nabla \cdot D \nabla \phi &= \sigma_t \left(\frac{\partial^2 \phi}{\partial x^2} + \frac{\partial^2 \phi}{\partial y^2} + \frac{\partial^2 \phi}{\partial z^2} \right) \\ &+ \sigma_{l-t} \left(\sin^2\theta \cos^2\varphi \frac{\partial^2 \phi}{\partial x^2} + \sin^2\theta \sin^2\varphi \frac{\partial^2 \phi}{\partial y^2} + \cos^2\theta \frac{\partial^2 \phi}{\partial z^2} \right. \\ &+ 2 \sin^2\theta \sin\varphi \cos\varphi \frac{\partial^2 \phi}{\partial x \partial y} + 2 \sin\theta \cos\theta \cos\varphi \frac{\partial^2 \phi}{\partial x \partial z} \\ &+ \left. 2 \sin\theta \cos\theta \sin\varphi \frac{\partial^2 \phi}{\partial y \partial z} \right). \end{aligned} \tag{22}$$

Alternatively, equation (21) can be simplified by taking an average of the source term over a small volume, and transforming the resulting equation by the Gauss equality to give

$$\int_v \nabla \cdot D \nabla \phi \; dv = \oint_S (D \nabla \phi) \cdot dS = \oint_S (\sigma_n |\nabla \phi|) dS, \tag{23}$$

where σ_n is the conductivity in the direction of the surface normal. The computation of the source term is described in detail in Publication V.

From the cable equations, it follows that the propagation velocity of an action potential is proportional to the square root of conductivity. This also holds for the generalized cable equation (21). The model should thus reproduce the theoretical ratio of propagation velocities:

$$\frac{v_{ax}}{v_{tr}} = \sqrt{\frac{\sigma_{ax}}{\sigma_{tr}}}. \tag{24}$$

Propagation velocities $v_{ax} = 0.7$ m/s and $v_{tr} = 0.3$ m/s, and conductivities like $\sigma_{ax} = 2.4$ S/m and $\sigma_{tr} = 0.4$ S/m have been reported in the literature [113, 45, 18, 10].

3.5 Volume conductor models

The human body does not resemble any simple geometric shape (sphere, spheroid, cylinder) that would allow for easy computation of the fields generated by the sources described earlier. Moreover, the body is highly inhomogeneous in the sense of conductivity, making the use of simple models even more unjustified [99]. There are several different methods of describing the complex shape and inhomogeneities of the human body in a computationally feasible way. These include

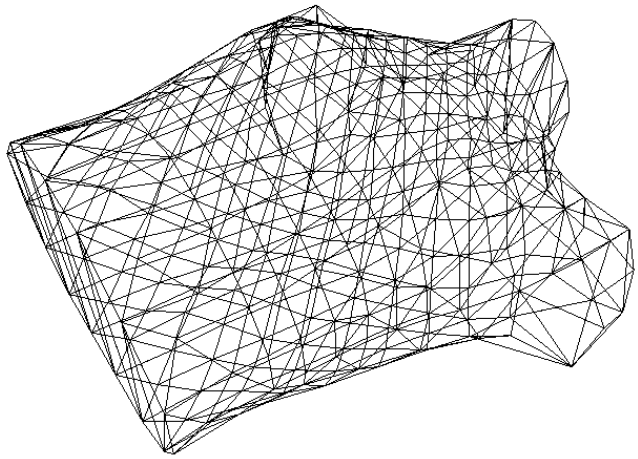

Figure 6: *The standard torso. The surface of the thorax has been described with 352 nodal points and 700 triangles. For visualization purposes, a recorded potential distribution from 120 electrodes needs to be interpolated to 352 the nodal points.*

the finite element method (FEM), the finite difference method (FDM) and the boundary element method (BEM). All of them have been used in the field of bioelectromagnetism, and the following description is related to the boundary element model. Straightforward application of the finite difference method requires the use of powerful computational facilities with substantial memory capacity, whereas the boundary element method is computationally lighter. However, the boundary element method is theoretically more complex [82].

The homogeneous infinite volume conductor model is the simplest way of computing the fields of a current source, because both the forward and inverse problems of electrocardiography have unique analytical solutions for simple source models like the dipole, provided that the measurement data are accurate. Although simple, this volume conductor model is the basis for solutions using more complex models incorporating inhomogeneities.

When accurate source location is required, inhomogeneus volume conductor models are used, incorporating the conductivity regions defined by the body surface and, e.g., the lungs and the blood masses of the heart. It has been found that the heart, the subcutaneous fat and the lungs have a significant effect on the body surface potentials, but even more importantly, the position and orientation of the heart needs to be correct. In fact, translation of 20 millimeters or a rotation of 15 degrees of the heart is equivalent of neglecting all the torso inhomogeneities in the computation of the extracardiac electromagnetic fields [11].

In the boundary element method (BEM), the surfaces are usually triangularized to achieve discretization of the problems, and the conductivities within each region are assumed to be homogeneous. One example of the triangularization of the body surface is presented in Fig. 6, showing the triangle mesh of a so-called standard torso used at Dalhousie University and Helsinki University of Technology. Currently, the most accurate way of obtaining the BEM models for inverse computations is to create an individualized torso model from the data acquired with magnetic resonance imaging (MRI). The anatomical images are first segmented to identify the boundaries of different organs included in the model, e.g., the heart and the lungs. After segmentation, the surfaces are triangulated to be used in the BEM calculations [80].

3.6 Boundary element formulation of the forward problem

The computation of the electric and magnetic fields, when the sources in the heart that generate the fields and the conductivity distribution of the thorax are known, is usually referred to as solving the forward problem of electro- and magnetocardiography. In an infinite homogeneous medium, the electric potential is given by

$$\phi_\infty(\vec{r}) = -\frac{1}{4\pi\sigma}\int_{v'}\frac{\nabla'\cdot\vec{j}_p(\vec{r}\,')}{|\vec{r}-\vec{r}\,'|}\,dv' \tag{25}$$

and the magnetic field by

$$\vec{B}_\infty(\vec{r}) = \frac{\mu_0}{4\pi}\int_{v'}\frac{\nabla'\times\vec{j}_p(\vec{r}\,')}{|\vec{r}-\vec{r}\,'|}\,dv', \tag{26}$$

where j_p is the primary current distribution already appearing in Eq. (7) [103, 100]. The conductivity differences in the human body cause accumulation of charge on these interfaces, which act as secondary sources of the electric field and affect the magnetic field through altered volume current distribution. These secondary sources are single-layer sources, the potential of which is already presented in Eq. (10). To evaluate the effect of conductivity boundaries, the interfaces are tessellated to surface elements S_k, and, in the discretization, the electric potential is assumed to be constant on each S_k. After the contribution of the secondary sources, it can be shown that the electric potential distribution on the boundaries is obtained from the integral equation [3]

$$(\sigma_l^i+\sigma_l^e)\phi_l(\vec{r}) = 2\sigma_n\phi_\infty(\vec{r}) - \frac{1}{2\pi}\sum_{k=1}^{M}(\sigma_k^i-\sigma_k^e)\int_{S_k}\phi_k(\vec{r}\,')\,\frac{d\vec{S}_k\cdot(\vec{r}-\vec{r}\,')}{|\vec{r}-\vec{r}\,'|^3}, \tag{27}$$

where M is the number of conductivity interfaces, σ_j^i and σ_j^e are the conductivities inside and outside the boundary surface element S_k, and σ_n is the conductivity of Eq. (32), i.e., the conductivity at the source location. Using Eq. (27), it can be shown that the magnetic field is [51]

$$\vec{B}(\vec{r}) = \vec{B}_\infty(\vec{r}) - \frac{\mu_0}{4\pi}\sum_{k=1}^{M}(\sigma_k^i-\sigma_k^e)\int_{S_k}\phi_k(\vec{r}\,')\,\frac{d\vec{S}_k\times(\vec{r}-\vec{r}\,')}{|\vec{r}-\vec{r}\,'|^3}. \tag{28}$$

Equation (27) above is analogous to Eq. (14), which shows that the secondary sources are indeed surface sources. It is also interesting to notice that the effect of a conductivity boundary to the solutions is dependent on the conductivity difference $\sigma_k^i-\sigma_k^e$ in Eqs. (27) and (28), as of course should be. To compute the potential, Eq. (27) can be discretized to obtain [51, 100]

$$\phi_l = g_l + \sum_{k=1}^{M}\omega_{lk}\phi_k, \quad l=1,\ldots,M. \tag{29}$$

In the previous equation, ϕ_l and g_l are discretized vectors from $\phi(\vec{r})$ and $2\sigma_n\phi_\infty(\vec{r})/(\sigma_l^i+\sigma_l^e)$, and $\omega_l k$ consists of the intertriangle solid angles multiplied with a constant depending on the conductivity difference on each boundary l. The magnetic field can also be obtained by discretizing Eq. (28):

$$\vec{B}_l = \vec{B}_{\infty,l} - \frac{\mu_0}{4\pi}\sum_{k=1}^{M}(\sigma_k^i-\sigma_k^e)\sum_{j=1}^{n_k}\phi_{l,j}a_j\frac{\vec{n}_j\times(\vec{r}-\vec{c}_j)}{|\vec{r}-\vec{c}_j|^3}, \tag{30}$$

where n_k is the number of triangles on the boundary S_k and a_j is the area of the j th triangle.

The primary current can be obtained from bidomain simulations of propagated excitation under the assumption of equal anisotropy ratios directly from the gradient of the transmembrane potential by [20, 74]

$$\vec{j}_m = \nabla \cdot D_i \nabla \phi_i = \nabla \cdot (D_i \nabla \phi_m + D_i \nabla \phi_e) \approx -\nabla \cdot D_i \nabla \phi_m. \tag{31}$$

This primary current can be used in the forward computations [96].

In the forward computations carried out this thesis, the ventricles were assumed to be embedded in a torso-shaped piecewise homogeneous volume conductor, including the lungs and the intracardiac blood masses. The infinite medium potential ϕ_∞ was determined from the discretized equation

$$\phi_\infty = -\frac{\sigma_1}{4\pi\sigma} \int_V \frac{\nabla v \cdot \vec{r}}{r^3} dV - \frac{\sigma_2}{4\pi\sigma} \int_V \frac{\vec{a}_3 \vec{a}_3^T \nabla v \cdot \vec{r}}{r^3} dV, \tag{32}$$

where V is the ventricular volume, v is v_m from Eq. 21, $\vec{a}_3$ is the local direction of the fiber axis, σ is the thorax conductivity ($\sigma = 2.0$ mS/cm), σ_1 is the transverse conductivity ($\sigma_1 = 0.5$ mS/cm) and σ_2 is the difference between the axial and transverse conductivity ($\sigma_2 = 1.5$ mS/cm) [96]. The first term of the potential in Eq. (32) represents the contribution of the isotropic component and the second term accounts for the anisotropic properties of the cardiac tissue.

The extracardiac magnetic field, $\vec{H}_\infty$, is evaluated from a corresponding equation,

$$\vec{H}_\infty = -\frac{\sigma_1}{4\pi\sigma} \int_H \frac{\nabla v \times \vec{r}}{r^3} dV - \frac{\sigma_2}{4\pi\sigma} \int_H \frac{\vec{a}_3 \vec{a}_3^T \nabla v \times \vec{r}}{r^3} dV. \tag{33}$$

To compute the body surface potential in the inhomogeneous torso, a "fast forward solution" is used:

$$\phi = (I - W)^{-1} \phi_\infty, \tag{34}$$

$$\vec{H} = \vec{H}_\infty + \vec{A}(I - W)^{-1} \phi_\infty. \tag{35}$$

In Eqs. (34) and (35), I is the identity matrix, W is a geometry matrix consisting of the solid angles subtended by a surface element at each node, and $\vec{A}$ is a vector-value geometry matrix taking into account the influence of the conductivity change surfaces on the magnetic field [100].

The subcutaneous skeletal muscle layer introduces an anisotropic domain into the volume conductor [11]. This anisotropy affects the computations of the electric potential. The anisotropy of the volume conductor can be estimated by the thorax extension method [78]. In this method, the outer surface of the volume model is uniformly inflated by a couple of centimeters to model the lower conductivity of the skeletal muscles in the direction of the surface normal.

4 Body Surface Potential Mapping

4.1 The electrocardiogram and the magnetocardiogram

The electrocardiogram, or the ECG, is a time-dependent potential signal created by the activating cardiac muscle and recorded at one location on the body surface against a reference. For clarity, the signals recorded invasively, e.g., on the surface of the heart are called electrograms. Usually, the so called Wilson Central Terminal (WCT) [142] is used to form the ECG reference.

In a clinical setup, the standard way of recording the ECG is to attach three limb electrodes, and six electrodes on the precordial area along the fourth intercostal line. The WCT is computed as an average of the potentials of the three limbs: the right and left arm and the left leg. The right leg is usually used to equalize the potential between the recording equipment and the patient. With this setting, the so-called twelve-lead ECG can be recorded. The leads I, II and III are potential differences between the limb electrodes, the so-called augmented limb leads *aVR*, *aVL* and *aVF* are the potentials of each limb lead recorded against the average of the potential of other limb leads (equal to being recorded against the WCT and multiplied by $\frac{3}{2}$), and the leads $V1$—$V6$ are the chest leads, also recorded against the WCT (see Fig. 7).

Different cardiac diseases may cause the ECG to distinctively deviate from the normal morphology. The deviations can be used to diagnose and characterize these diseases. For example, the ischemia caused by the coronary artery disease (CAD) manifests itself as a baseline deviation of the S to T segment of ECG, usually referred to as ST depression or elevation. On the other hand, a patient having an accessory conduction pathway between the atria and the ventricles in Wolff-Parkinson-White syndrome has a so called delta wave preceding the R wave. Finally, patients having myocardial infarction or ventricular tachycardia show a totally different morphology of the ECG than normal subjects [44].

In the body surface potential mapping (BSPM), from 32 to as many as 256 ECG electrodes are simultaneously registering the potential field created by the beating heart [53]. Body surface potential mapping, also called ECG mapping, can be viewed as an extensive ECG only, but BSPM is more correctly described to be a method that yields the time-depedent potential distribution created by the activating cardiac muscle, recorded on the whole thorax with a large number of electrodes.

Figure 7 shows the ECG signals recorded by a 120-channel BSPM device, with 9 leads of the standard 12-lead ECG displayed separately on the top. The figure illustrates that the standard 12-lead ECG in this case is a small subset of the potential signals recorded by BSPM. In fact, the BSPM recordings are usually visualized in a different way that describes the potential distribution on the thorax more clearly (see Fig. 6).

4.2 Recording hardware and software

The body surface potential mapping system used in this work has 120 channels and has been designed to be used in clinical work, e.g., during catheterization [121]. Below, a more detailed

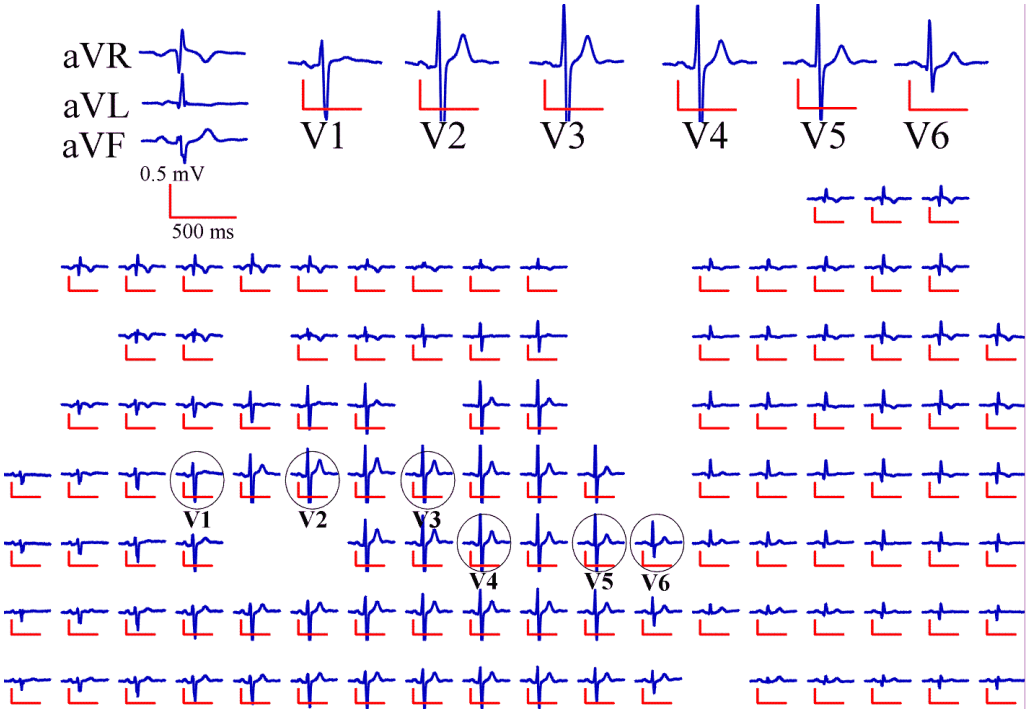

Figure 7: *The relation of 12-lead ECG to body surface potential mapping. Nine of the 12-lead ECG leads form a small subset of the 120 BSPM leads. Some of the leads are not displayed because of inferior signal quality. Due to the redundancy, the interpretation of the BSPM does not suffer from omitting some bad channels to the extent the 12-lead ECG would. Fig. 9 presents the electrode layout.*

description of the system is given. To date, the BSPM system has been used in several hundreds of patient recordings covering most common cardiac diseases like the ischemic heart disease [39, 40, 133], ventricular and supraventricular arrhythmias [118, 120, 119, 121].

In the body surface potential mapping equipment used in this work, there are separate amplifiers and filters as well as analog to digital conversion circuits for each channel. These parts form the channel units that are positioned on a motherboard that takes care of the multiplexing and synchronization of the channels. In the patient front-end, the digital data are converted to an optical signal that is transmitted to the computer [90]. In the computer, the signal is converted back to digital form and buffered for acquisition to the computer memory.

The electrodes of the system used in this work are attached on flexible strips with an interelectrode distance of 50 mm. The strips are positioned on the body surface according to Fig. 9. The level of the fourth intercostal space used in standard 12-lead electrocardiography has been adopted for a reference level, and the strips are aligned vertically on the body surface. The positioning of the electrodes is similar to that used in Dalhousie University [94], which makes easy interpretation of the data possible also in other scientific centers.

The data acquisition program used in this work was designed for ease of use in a clinical setup. When the program is started, it checks the optical connection to the patient front-end. If something is wrong, an error message is given, and the user is allowed to continue when the system is powered on and the optical link is established. At this point, the user is immediately presented with a screen where the current signal on the ECG limb leads and leads V1–V3 are shown. The user can easily

browse through the strips confirming the signal quality on all channels. After quality control, the user will have to enter the patient and session information before the recording can be started. The recording is then started by pressing a button on the screen.

4.3 General analysis methods for body surface potential mapping

The main advantage of body surface potential mapping, compared to 12-lead ECG, is the ability to present the cardiac potential distribution on the whole thorax. The program for isocontour visualization features the creation of several different types of maps. Currently, the program allows the creation of maps at a chosen time instant (instantaneous maps), maps at succesive time instants (sequential maps), maps of an average potential over a time interval (e.g., QRS mean integral maps), and maps of the difference between two potential maps (departure maps). The calculated maps or sequences can be saved to a file for further analysis or for comparison to other maps. The saved maps can be loaded back to the program, and they can then be selected for display from the menu.

Before the calculation of maps, a baseline must be set. This is done by selecting an interval from the data, usually before the QRS complex, over which an average is calculated to obtain the baseline on each channel. The selection can be done by an expert, or an automatic method can be applied [69]. In either case, the baseline in a rapid VT is still ambiguous, because no isoelectric time interval is available. Therefore, alternative methods for the creation of maps have been proposed in Publication II.

The presentation of the data on a three-dimensional surface with good enough spatial resolution requires interpolation. A method based on the minimization of the surface Laplacian was chosen for this purpose [101]. The matrix operations required for the calculation of the surface potential at all nodes of the triangulated body surface have to be performed only once. Thus the interpolation only involves one matrix multiplication at the time of map creation, if the set of known potential values remains the same.

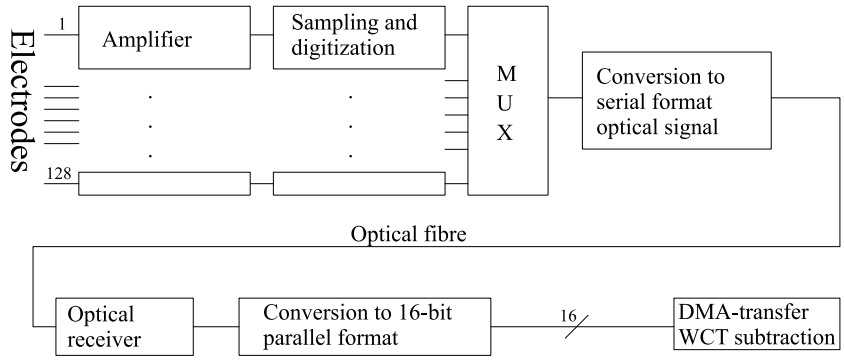

Figure 8: *The hardware organization of the body surface potential mapping system. All the patient front-end electronics are commercially manufactured, whereas parts of the digital data acquisition electronics have been developed in earlier work by the author [121].*

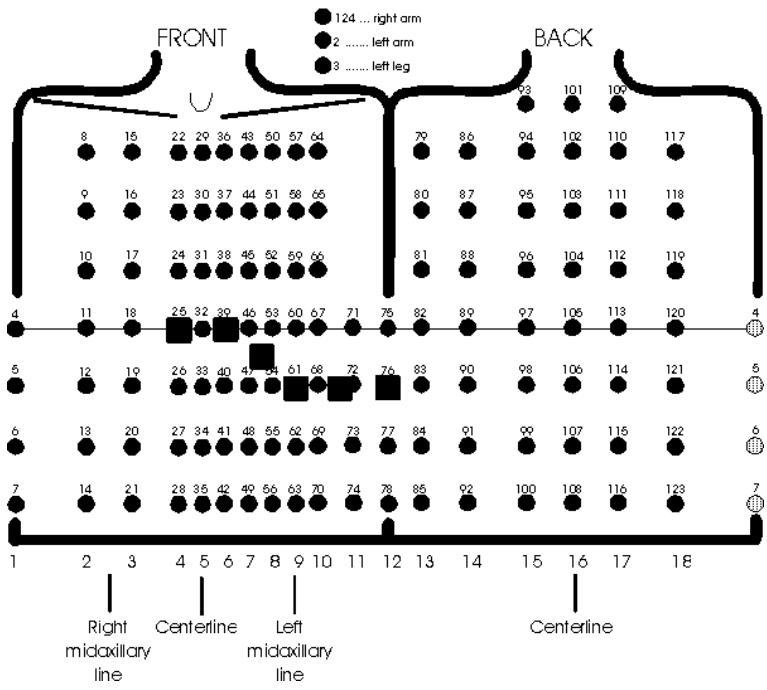

Figure 9: *Electrode positioning on the body surface. The fourth intercostal line has been drawn to the figure as well as other anatomical landmarks used in electrode positioning. The electrode positioning was adapted from the layout used in [94].*

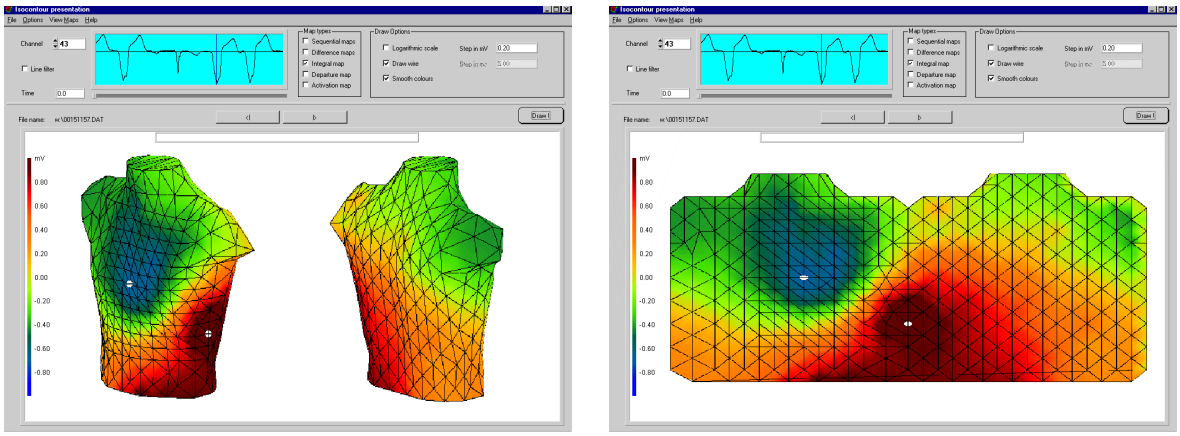

Figure 10: *Visualized potential maps of the BSPM signals. The program is designed to plot potential distributions on the standard torso as three-dimensional (upper panel) or two-dimensional (lower panel) images. The triangular mesh used in the plotting is not restricted to the standard torso. Interpolation of the potential signal is performed before plotting [101], as well as per channel baseline correction and possible 50 Hz filtering.*

4.4 Arrhythmia risk assesment

Several methods have been proposed for detecting the vulnerability to life-threatening arrhythmias from body surface potential mapping and magnetocardiographic mapping signals [39, 40]. In such methods, the temporal signals on each channel are analysed by advanced signal processing methods: averaging, late potential analysis, spectral turbulence analysis, QRST integral analysis and spatial parameter maps. The use of the parameters is discussed in detail in Publication III. In electro- and magnetocardiographic mapping, compared to 12-lead ECG, there are more signals available for analysis, which calls for automated signal processing methods but also makes the methods more robust to channel failures. The measured signal could also be more robust against interindividual variations in geometry. Individual rotation or translation of the heart in relation to the thorax from the average anatomy does not affect the outcome of the analysis greatly, since the method always uses the most prominent leads for analysis based on the actually recorded signal.

In Publication IV, the utility of magnetocardiographic mapping, body surface potential mapping and Frank lead signal-averaged ECG was investigated in patients with previous myocardial infarction. The following time domain analysis parameters were used for the electrocardiographic methods: QRS duration, rms amplitude during the last 40 ms of the QRS complex and the duration of the low amplitude signal below 40 μV. Corresponding parameters were computed for the z-components of the magnetic field from MCG. MCG and BSPM showed high correlation in parameter values, whereas the SA-ECG parameters were complementary to the MCG parameters. All methods performed equally well in identifying the risk for arrhythmias.

4.5 Localization by BSPM map analysis

Interpretation of the BSPM signals

The localization of arrhythmia sources during catheterization is usually based on the use of previously recorded [125, 126] or precomputed [58] databases or deductive methods like those used in vectorcardiography. These methods are based on the assumption that a monomorphic and stable tachycardia originating from the same area of the heart will produce similar time dependent potential distribution patterns on the body surface for every patient [125, 126]. This assumption is not strictly valid, but the localization accuracy has proven to be sufficient for clinical use [123, 124]. On the other hand, the classification accuracy of the decision trees for standard 12-lead ECG is between 80 and 90 % [64, 50, 73].

Localization of origins of tachycardias

For the localization of VTs, the ECGs obtained during an episode of tachycardia are averaged at each channel, over the time interval from the Q-wave onset to the S-wave offset (QRS integral [55, 94]), and the resulting figures are plotted as a distribution on the body surface (see Fig. 12). Essentially, this method will result in the visualization of the R-wave direction and strength on the body surface. Several databases of body surface potential map patterns have been published that can be used for the localization of ventricular arrhythmia sources with and without myocardial infarction [125, 126, 123, 124, 70, 107] and for the localization of supraventricular arrhythmia sources [8]. Such localization makes use of known landmarks and agreed segmentation of the human ventricles [64, 63, 15].

Clinical electrophysiologic testing, i.e., an electrophysiologic study (EPS), is a standard method to investigate the electrophysiologic condition of the heart. In this method, catheters are inserted into the heart, and electrograms are recorded from the endocardial surface with the aid of an electrode attached to the catheter tip. The method yields information about the electrical activation of the cardiac muscle. The localization of arrhythmia sources is usually done with this method before any interventions [141, 148].

In the EPS, the aims for studying patients who have had sustained ventricular tachycardia are 1) to rule out other diseases, 2) to induce the tachycardia, and 3) to localize the tachycardia source. Usually, three multipolar pacing and recording catheters are used. First, the catheters are positioned via the femoral vein to the right ventricular apex, the right atrium and near the bundle of His. After supraventricular mechanisms of arrhythmia have been ruled out, the tachycardia is induced with ventricular pacing and programmed extrastimuli at driving cycles of 600 ms and 400 ms. The pacing is first done from the right ventricular apex and then from the right ventricular outflow tract, if needed. Left ventricular pacing is only rarely used to induce the arrhythmia. If the arrhythmia is not inducible, isoprenaline is sometimes used to provoke the arrhythmia, especially in patients without structural heart disease.

The clinical procedure of the electrophysiological study is essentially unaltered by the addition of BSPM. Before the EP study and ablation procedure, a baseline recording is made. This is a recording lasting at least one minute while the patient is at rest and under no influence of any antiarrhythmic medication. During the first interventional step, a tachycardia is induced by programmed stimulation so that the morphology of the induced VT is similar to that of a previously recorded sustained VT [140, 65]. If this step is succesful, the tachycardia is recorded by the BSPM for localization. In case this localization is for some reason inaccurate, additional recordings are taken during cardiac pacing. The recordings are compared successively to find a match to the patient's tachycardia recorded before the ablation procedure. Whether it is tachycardia itself or response to pacing that is recorded, usually at least 20 seconds of it is captured when the patient is hemodynamically stable. After a successful ablation of the arrhythmia, it is customary to continue the procedure for half an hour to see whether the tachycardia is still inducible. After the treatment has been confirmed to be succesfull, a post-treatment BSPM recording of at least one-minute duration is made. The course of a BSPM assisted catheter ablation procedure is outlined in Fig. 11.

After BSPM localization of the arrhythmia source, the standard clinical catheter localization procedure is followed. There is no clear rule how long the pacing phase should be continued, but usually the localization from even a few pacings can guide the catheter close enough to the arrhythmia source. The principal criteria for localization with the catheter are [93]:

1. Earliest local activity during tachycardia or continuous diastolic activity.

2. Matching of the QRS morphology of the tachycardia with the morphology produced with pacing at the presumed site of origin of the arrhythmia.

3. Succesfull entrainment of the tachycardia with pacing, i.e., the cycle of the tachycardia can be shortened with pacing without changing the morphology.

Points 1 and 2 represent the exit site for re-entry and point 3 the slow conduction zone of the re-entrant circuit.

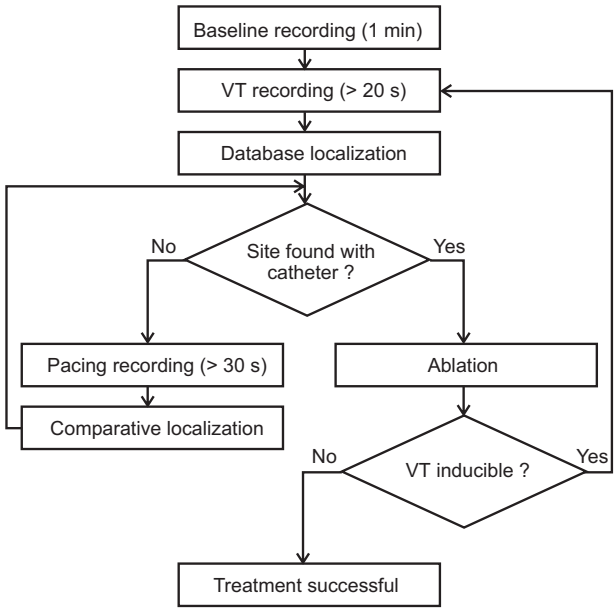

Figure 11: *Diagram of VT localization by BSPM and pace mapping. First, the QRS integral map from induced VT is compared to a database. Then, if the arrhythmia source is not found, the exact location of the origin is found by matching the map from ventricular pacing to the VT map.*

After catheter localization, radiofrequency (RF) electrical current at the power of 10-50 W is applied to the site for up to 60 seconds. If the treatment is not successful, the search of the effective site is continued and ablation is repeated until the tachycardia terminates. A successful ablation is considered as clinical proof of the correct localization.

Localization by BSPM is confirmed when the clinician has found early electrical activation from the site pointed to by the method. This indicates that the endocardially recognizable signal is also identifiable on the body surface, and the cardiac activation created by the extraneous activity takes place without spreading to the conduction system. On the other hand, the confirmation to the result of an electrophysiological study is the succesful ablation of the arrhythmogenic tissue. This criterium was presented already by Mines [93]. However, the localization results from the EPS may differ significantly from the result given by BSPM. Thus, occasionally BSPM localization can be confirmed, but the result of the electrophysiological study cannot.

Following the EPS protocol, a crude localization is first made from the 12-lead ECG and from the intracardiac recordings of the atria. Then mapping with the ablation catheter is performed. For an arrhythmia originating in the left atrium, a transseptal puncture is needed. The earliest local activity shows the site of origin of the arrhythmia, but entrainment with pacing can also reveal the slow conduction zone, as it does in ventricular tachycardia [30].

The localization of atrial tachycardias by BSPM follows similar guidelines as the localization of ventricular tachycardias (see Fig. 13). The activation pattern in the atria during atrial tachycardias is more complicated than ventricular activation patterns. The activation is fragmented due to the complex geometry of the atria. Besides, the fundamental principles of genesis of atrial tachycardia are not well understood. However, interpreting the P-wave potential pattern similarly to QRS mean integral interpretation yields promising results in the case of focal and re-entrant atrial tachycardias that originate from a small area of slow conduction. [122]

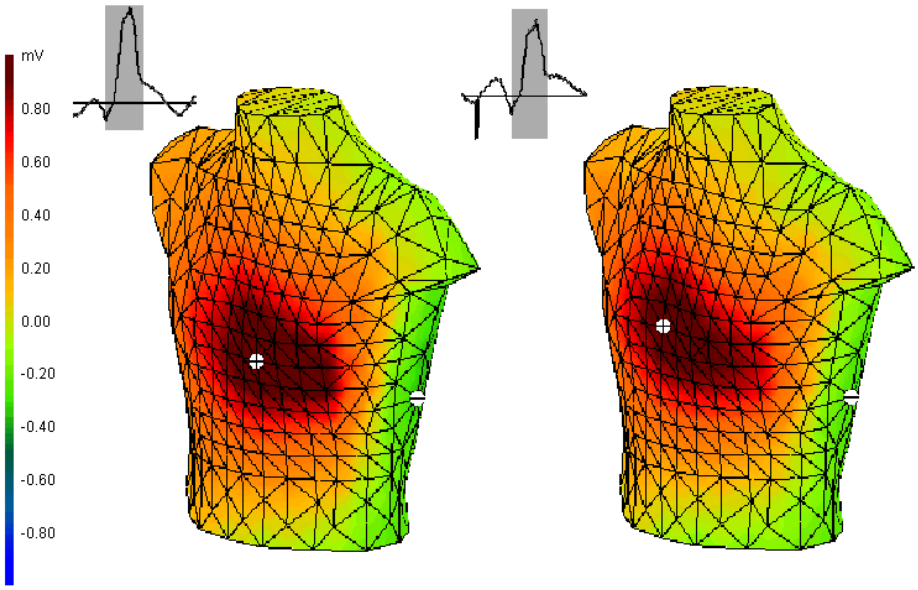

Figure 12: *VT localization by pace mapping. The figure shows a QRS mean integral map over the shaded area during induced VT (left) and ventricular pacing (right). The morphology of the map is strongly modified by a substantial aneurysm in the left ventricle. Initially, the tachycardia was localized by the database to posteroseptal basal region of the LV, but by pace mapping the source of tachycardia was found to be in the posteroseptal apical left ventricle.*

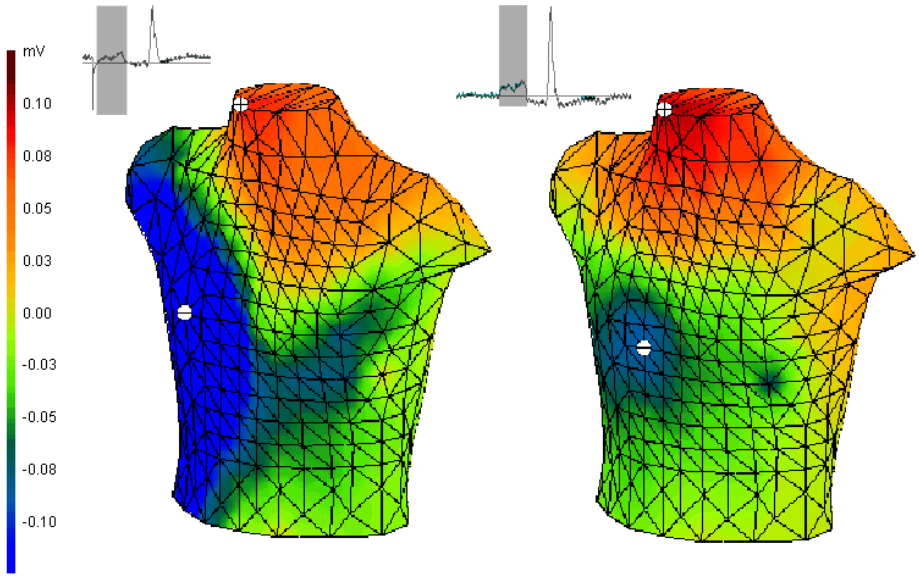

Figure 13: *Localization of atrial tachycardia by pace mapping. The P-wave integral maps (shaded regions) from pacing and spontaneous atrial tachycardia are matched in a similar fashion to the localization of VTs by pace mapping. Recently, a database has been published presenting the different map morphologies obtained by pacing from different locations in the atria [122]. The origin of the atrial tachycardia was found to lay anterolaterally in the low right atrium.*

Localization of an accessory pathway

An anterogradely conducting accessory pathway (AP) manifests itself in the ECG as a delta wave before the QRS complex. The location of the pathway can be found by comparing the patient's delta wave map (see Fig. 14) to the distinctive patterns generated by different locations of the accessory pathway. The pattern of the T wave can also be used for localization. Normally both methods are used to confirm the location [8, 13, 27, 36, 67, 77, 114]. If the delta wave is poorly distinguished during the sinus rhythm, it is possible to pace the heart from the atrium to induce ventricular pre-excitation via the accessory pathway.

The ablation catheter is positioned to the site of the earliest ventricular activity, the insertion site of the accessory pathway in the ventricle, or in the coronary sinus. Another possibility is to identify the earliest atrial activity in the atrium during orthodromic tachycardia or ventricular pacing when the conduction in the accessory pathway takes place retrogradely from the ventricular to the atrial side. The final proof of pathway localization is the disappearance of conduction in the accessory pathway after radiofrequency ablation. This manifests itself as a loss of the delta wave and elimination of the arrhythmia circuit.

The standard 12-lead ECG is an efficient tool for the localization of WPW accessory pathways, but it frequently fails in predicting correctly the location of septal pathways. However, the accuracy of body surface potential mapping yields more reliable results in this clinically important case. Using the BSPM, it is possible to localize the insertion site of the pathway to the ventricles to either right or left ventricle. This makes is possible to reduce the number of catheters used or to avoid a transseptal puncture, which is often used in the case of left-sided pathways that are difficult to localize.

Ischemia classification by body surface potential mapping

Ischemia in the cardiac muscle causes the magnitude of the action potential to diminish locally. This results in a drop of the intracellular potential during the plateau phase of the action potential, which is seen on the body surface as negativity during the ST-interval. On the other hand, if the ischemia is transmural, the state manifests itself as a positive potential on the body surface. The confined deflection from the zero line during the ST-segment is thus a clear indication of ischemia, and the location of the changes on the body surface reflect the location of the ischemia in the heart.

Ischemia develops in the heart, e.g., during physical load in the supply area of a coronary artery with a stenosis, when the flow in the vessels supplying blood to the cardiac muscle is partially obstructed by the increased pressure generated by the muscle (supply ischemia). If the demand for oxygen increases in the cardiac muscle due to increased workload beyond a level that can be sustained by the coronary arteries, demand ischemia develops. [31, 68, 39]

The standard way to induce ischemia to detect coronary artery disease is to use an ergometer. Usually, the ergometer is a bicycle that is pedalled in vertical position while the standard 12-lead ECG is recorded. However, for the purpose of MCG and BSPM stress testing, a more suitable non-magnetic stress ergometer has been constructed, which is pedalled in supine position [133].

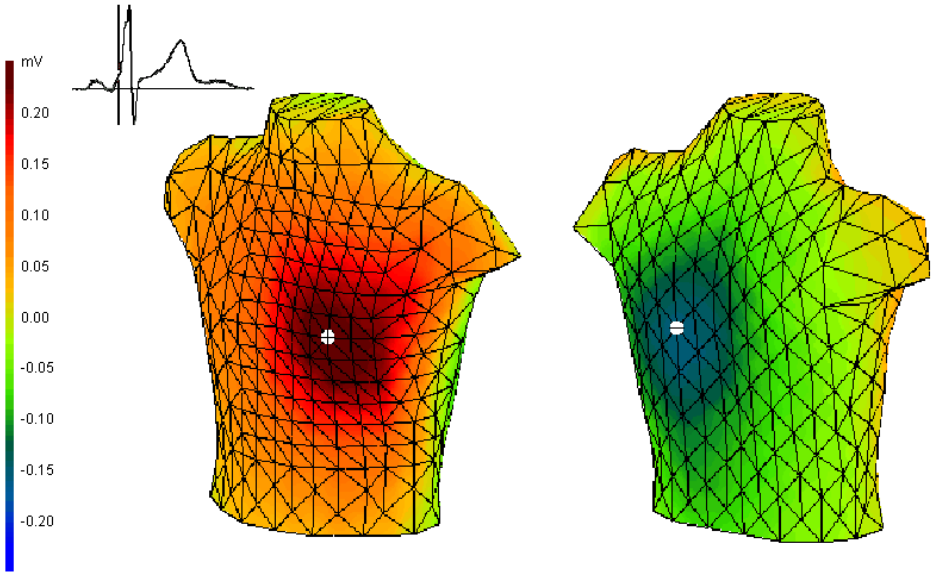

Figure 14: *Localization of the accessory pathway in the Wolff-Parkinson-White syndrome using BSPM. Like in the localization of the origin of ventricular tachycardia, maps plotted during the premature activation (delta-wave in the ECG) present characteristic features according to the pre-excitation site. The figure presents a delta-wave map plotted 60 ms after QRS onset (vertical line), localizing the pathway to the lateral LV on the atrioventricular ring.*

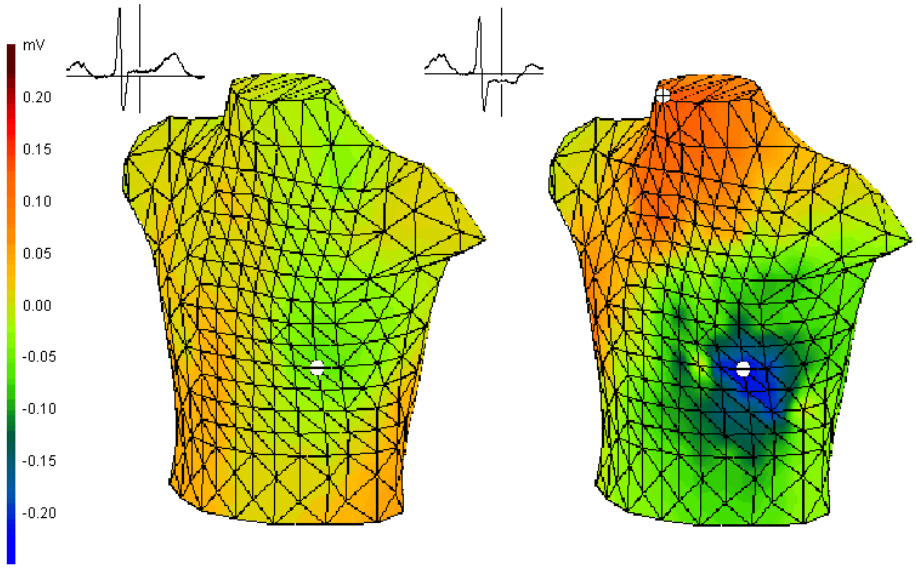

Figure 15: *ST-segment changes in the BSPM, induced in ergometry. The patient had a narrowing in the proximal LAD and developed chest pain during the ergometry. The angiographic findings support the changes seen in the above body surface potential map.*

During the stress testing, the patient is working against a calibrated external load that is increased gradually until the patient's heart reaches a certain limit for the heart rate, or the patient experiences disturbing chest pain. The changes in electrophysiology are visible best one to four minutes after the cessation of pedalling, and their morphology on the body surface reveals the location of the narrowing in the coronary artery (see Fig. 15) [39].

To treat ischemia in coronary artery disease, percutaneous transluminal coronary angioplasty (PTCA) is nowadays frequently used instead of the coronary bypass surgery, if the narrowing of the artery is well confined. In PTCA, a balloon is inserted to the coronary artery at the location of the stenotic occlusion, and is then inflated to expand the artery. During the inflation, the cardiac muscle develops a strong but reversible ischemia from a well-defined occlusion. This makes the PTCA a good tool for investigating acute supply ischemia, because the influence of occluding different parts of the coronary arteries can be studied individually. This kind of data are essential for the development of ischemia localization methdods for BSPM.

Body surface potential mapping has also been shown to be superior to 12-lead ECG in detecting acute and old infarctions [39, 40]. The ability of BSPM stems from the distribution of electrodes, whereby it is likely that always some electrodes are be sensitive to pick up the indicators of ischemia. ST-level, ST-slope, ST-integral and T-integral maps have been used for ischemia detection.

4.6 Localization by self-organizing maps

Publication I presents localization of sources of ventricular tachycardia using self-organizing maps (SOMs). We trained a Kohonen self-organizing map [71] with body surface potential maps obtained during pacing from 18 patients, altogether several hundred different potential maps. The maps were obtained by selecting a representative QRS complex together with the baseline chosen beforethe QRS onset. The selected QRS complexes were then sampled at 5 ms sampling interval and suitably rescaled. The SOM then organized to comprise 12x16=192 codebook BSPM maps (see Fig. 16).

When a new potential map is presented to the trained SOM, the best matching node is searched. Tracing the best matching nodes for potential maps during a QRS complex of a VT results in a trajectory on the SOM units, as shown in Fig. 16. For multiple different VT source locations, a database of trajectories was created. The trained SOM was finally tested at six independent BSPM recordings by comparing their trajectories to those of the database trajectories. The results of this method can be evaluated against two criteria: the SOM has organized itself in a reasonable manner, i.e., the adjacent cells resemble each other; 2) the QRS trajectories provide sufficient information for reliable localization of ventricular tachycardias.

A codebook BSPM map on the trained SOM map can be interpreted as an integral map representing a VT starting from a certain site on the endocardium. The quality of the organization can be viewed using this criterium. In all teaching runs, the SOM organized to a good quality representation of the endocardium, i.e., adjacent points on the endocardium mapped to adjacent points on the SOM. Moreover, the SOM did not include any meaningless or random maps. Of all teaching runs, the SOM that resulted in the lowest quantization error (difference between the SOM codebook maps and input data) of the test set was chosen to be used in the classification.

Figure 16: *VT localization by trajectories on the self-organizing map. Plotting the best matching nodes on the SOM during the QRS creates trajectories describing the morphology of the VT (left). This can be used for the localization of arrhythmia sources by plotting trajectories from several different pacing sites and a VT time trace (black) on the previously taught SOM (right). [119]*

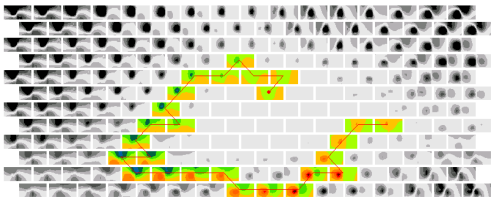

Figure 17: *Automated creation of SOM trajectories. The best-matching nodes are first located (some of the coloured maps), and then the trajectory is connected by interpolating the input data linearly between the time instants whose best-matching nodes are not adjacent on the SOM.*

The codebook organization could be further improved by using different distance measures, by changing the topology of the SOM, e.g., to three-dimensional, and by using better scaling of the codebook vector components. Especially the effect of scaling was found to be significant during the experiments. When the original 123-channel data were used, the SOM organized strongly according the patterns that were prominent on the precordial area, where the signals are large. When interpolated 352-channel data were used, the significance of the precordial leads was diminished, and more representative organizations of the SOM were achieved (unpublished observations).

The classification, i.e., VT localization, was done at the first stage by visual comparison of the trajectories from the test set with the trajectories in the comparison set. There were two pairs of similar VTs in the ramdomly selected teaching and test sets (see Fig. 16). The localization match was confirmed against QRS integral maps and clinical data, and in both cases the SOM method performed equally well as compared to the QRS integral method. Because of a small comparison set, the rest of the test set could not be localized well with either of the methods. Currently, automated creation of the trajectories is possible, as shown in Fig. 17.

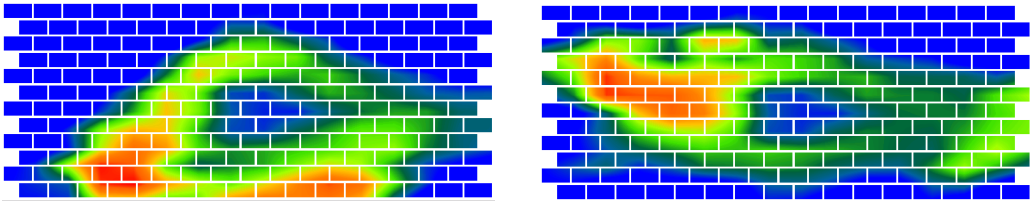

Figure 18: *Distance maps on SOM for VT localization by learning vector quantization. For each node on the SOM, the shortest distance between the codebook vector of that node and the data vectors during the QRS complex were calculated. After scaling, the distance distribution is plotted on the som, and forwarded to the LVQ classification procedure. Two figures of trajectories resulting from pacing in different sites are presented.*

The time tracings of the paced beats on the SOM were quantified for subsequent localization of the pacing site as follows: For each node of the SOM the shortest distance between the codebook vector associated with that node and the data vectors of the BSPM sequence were calculated. After logarithmic scaling a distribution of distances over the SOM is obtained. This distribution is in the following referred to as *QRS distance map*. Two QRS distance maps from different pacing locations are presented in Fig. 18: In the panels, bright nodes are closer to a particular BSPM data vector from the sequence than dark nodes. The distance maps of all paced beats are used as input for a LVQ classifier. In the LVQ algorithm, vector quantization is used to directly define the class borders according to the nearest-neighbor rule [72]. The accuracy of the LVQ classification depends on the number of codebook vectors assigned to each class as well as on the learning rate.

In the future, body surface potential maps used to teach the SOM could be obtained from simulations of ectopic activation in the heart model, perhaps with noise added to the maps to make the SOM organization more robust. This approach is feasible also in the sense that it can be used to generate a different set of data for creating the trajectories, whereby the two sets of data (training and testing) are statistically independent. Moreover, the geometry of the thorax can be varied to increase the variability in the training data.

5 Modelling of electrical activity in the heart

A ventricular model of the human heart that produces correct normal activation can be used, e.g., to simulate the effects of ischaemia and infarction [79, 26] or arrhythmias involving the conduction network [10]. Such a model must feature a realistic anatomical structure, including intramural fiber rotation, and a physiologically sensible model of the conduction process. Technically, simulations of the ventricular activation have become feasible with modern computing power. However, the scarcity of information on the anatomy of the conduction system and on the measured activation sequence of the human heart limits the accuracy of the models. [28, 127, 23, 24, 25, 134]

5.1 Computer models of cardiac activation

Cardiac activation has been modelled on several levels. Action potential models like the Beeler-Reuter model and the Luo-Rudy model aim at describing the ionic currents as accurately as possible. Such models can reproduce the action potential of a single cardiac cell very well, but with current computers, are still infeasible to be used in larger simulations. The properties of interconnected cells and slabs of cardiac tissue have also been studied [128, 112, 18, 46, 131], and these studies have revealed important properties that any realistic model must have: anisotropy due to fibrous structure, realistic fibre geometry and intramural fibre rotation and correct boundary conditions. Simulations in realistic heart models have made it clear that to reproduce correct activation of the normal heart and correct electrocardiographic signals, the model must feature realistic anatomy and fibre structure, have a proper conduction system and be anatomically correctly positioned withing a thorax model [91, 92, 105, 106, 74, 78, 95, 96, 9]. Such models can also be used to simulate activation in abnormal conditions [79, 146, 26, 10, 56].

Overview of cardiac modelling

Clayton provides an excellent review on cellular models and tissue models, ranging from the models describing the microscopic cell-to-cell couplings to whole-heart models [16]. Clayton considers the computational model to hold significant promise to supplement and replace clinical experiments in the future. He sees that there are, however, three major challenges in the adoption of these models. First, he emphasizes the correct selection of cell and tissue models depending on the application of the model. Second, he considers the geometry of the model to be important. Third, the computational power will always remain a challenge.

In a paper in 1993, Henriquez discusses the benefits and shortcomings of various models [45]. The bidomain model with equal anisotropy ratios in the intracellular and interstitial domains fails to predict correct behaviour in extreme conditions. Furthermore, these models do not predict the extracellular potential correctly, in fact, they assume it to be zero. Still, Henriquez hints to that the bidomain model may be modified so that it is able to produce some effects that the traditional bidomain model cannot, for example by adding discrete elements to mimick the behaviour of gap junctions or by incorporating directional differences to action potential shape.

Winfree discusses extensively the effects of choosing the diffusion coefficient D, i.e., the conductivities of any model of the myocardium [143]. Winfree relates the value of D to phenomena like ischemia, cell-to-cell decoupling, decay into fibrillation and re-entrant arrhythmias. In fact, the value of D is so crucial that it determines the validity of any continuum model. Yet, Winfree is of the opinion that monodomain models are probably accurate enough to determine activation patterns. He warns, however, that not just any conductivities should be accepted without questioning.

Action potential models

One of the fundamental action potential models was presented by Beeler and Reuter in 1977 [6]. The action potential model incorporates four ionic currents: the inward sodium current i_{Na}, a slow inward current i_s mostly carried by calcium ions, a time-dependent outward potassium current i_K, and a time dependent outward current i_{x_1} mostly carried by potassium ions. The model is computationally relatively light compared to more detailed models like the Luo-Rudy model [81]. The Luo-Rudy model is a model of the ionic currents of the guineapig heart. The model features more than fifteen ionic currents, also incorporating the currents of the sarcoplasmic reticulum. For the verification of these models, detailed descriptions on the measured ionic currents have been provided [14].

Shaw and Rudy simulated the effect of ischemic conditions on the cell-to-cell conduction using the Luo-Rudy model [117]. The simulations were carried out for a fiber of 70 serially arranged Luo-Rudy cells connected by gap junctions. They found out that applying realistic potassium concentration elevation, hypoxia and acidosis, a conduction block could be induced. Although it is currently infeasible to carry out this type of simulations in a whole-heart model, this work shows that it is possible to model real cardiac conditions arising from disturbances at the level of ionic currents.

Models of cardiac tissue and numerics

Roth has considered the effect of the boundary conditions on intracellular current by comparing two alternative formulations for the boundary condition [112]. The first condition proposed for the intracellular current is that it vanishes at the boundary to the extracardiac space, that is, the sealed-end condition. The second condition proposed for the intracellular current is that it is equal to the membrane current at the boundary. Roth found that the two boundary conditions give essentially equal results when the space constant is large compared to the cell size.

Colli Franzone *et al.* demonstrates the use of an eikonal model in slab simulations [18]. They used conductivity values of $\sigma_l^e = 2.0$ mS/cm, $\sigma_t^e = 1.3514$ mS/cm, $\sigma_l^i = 3.0$ mS/cm and $\sigma_t^i = 3.1525$ mS/cm, and $\chi = 2000\ \mathrm{cm}^{-1}$ and $C_m = 0.8\ \mu\mathrm{Fcm}^{-2}$ for the membrane properties. They claim to achieve comparable results than with, e.g., our model, without the limitation of equal anisotropy ratios. Using the eikonal model, Colli Franzone *et al.* were able to demonstrate that the depth of the initial stimulus can be deduced from the shape of the epicardial potentials [17]. Moreover, the importance of incorporating sources due to the anisotropy of the cardiac muscle was stressed, as this is the only way to explain non-zero potentials generated by a closed activation wavefront.

Taccardi *et al.* revisit the question of the effect of intramural fibre geometry on the propagation [131]. They found in their review that the most significant factors in cardiac activation are: the anisotropy due to the shape of the cardiac cells, rotation of the fibre direction from the epicardium to the endocardium, the obliqueness of the fibres compared to the epicardial surface, and the effect of the conduction system.

Roth provides a comprehensive study of different conductivity values reported for the bidomain conductivities [113]. The study points our a distinctive inconsistency in the measurement, thus virtually allowing the modeller to pick the conductivities to be used at will.

Plonsey *et al.* computed the current flow patterns in a two-dimensional slab under various conductivity conditions [104]. The results show, that the current flow patterns extend fairly far from the excitation wavefront. Furthermore, it is clear that the two-dimensional results can not be directly generalized from the one-dimensional case.

Spach *et al.* measured activation in specimens of cardiac tissue from 29 humans and evaluated the directional properties of the action potential [128]. Although traditional monodomain models do not predict differences in action potential shape attributed to the direction of propagation compared to the fibre direction, Spach *et al.* were able to observe such behaviour in real cardiac tissue. The observed differences in the maximum rate of change of the membrane potential during upstroke and the shape of the action potential foot were attributed to the membrane capacitance being dependent on direction of propagation. Capacitances of $1.0\ \mu\mathrm{F}/\mathrm{cm}^2$ and $0.5\ \mu\mathrm{F}/\mathrm{cm}^2$ were used to simulate propagation in the longitudinal and in the transverse direction, respectively. In a later paper, Spach *et al.* hypothesized that the cell-to-cell connections at the intercalated disks explain the differences in apparent directional capacitance and load observed by the cell [129].

In a paper in 1996, Henriquez *et al.* emphasize the importance of taking into account the extracellular potential [46]. Evidence in favour of direction-dependent rate of rise and action potential shape is presented, and these dependencies are attributed to the different loading conditions in different directions as well as the fibre rotation across the wall of the heart. Henriquez *et al.* investigated the differences in rate of rise and shape of the action potential comparing computations under the assumption of equal anisotropy ratios to computations with unequal anisotropy ratios. They found that in the presence of a bath, the action potentials in the case of unequal anisotropy ratios showed clear directional dependence, whereas in the case of equal anisotropy ratios they did not. Henriquez *et al.* consider the most important characteristics of any model of cardiac tissue to be the ability to reproduce effects due to anisotropy in both intracellular and extracellular regions, the presence of adjacent volume conductors, fiber curvature and fiber rotation.

Braun *et al.* present a numerically stable method for solving partial differential equations in a highly irregular and evolving grid [12]. The problems that are solved by this method may come up if movement is taken into account in the heart model and the activating elements are in relative movement. Some similarity between this method and the approach in our model can be seen. We have used an approach similar to Braun's natural-neighbour influence function in the calculation of the nodal excitation, where all neighbours of the cell are allowed to influence the potential change in the centre cell.

Harrild *et al.* describe a method for simulating cardiac conduction with a model that has an irregular grid [41]. They compute the changes in the potential of a cell by taking into account the

contribution of each 6 facets of the element, and using 18 points around each facet to determine the current flow through the facet. In this sense, the method is a lot like the one used in this work (Publication V), but is numerically much more demanding and perhaps also more accurate.

Barr *et al.* have computed the response of a two-dimensional excitable tissue slab to a stimulus slightly off the surface [4]. This simplified work shows one potential application of any heart model: the model can be used to predict responses to externally applied electrical current, which is important for modelling, e.g., defibrillator shocks.

Heart models

One of the fundamental works in cardiac modelling are the two papers by Miller and Geselowitz in 1978 [91, 92]. Their model incorporated 4000 activating elements and the current dipoles were lumped to 23 sum dipoles. Their action potential model is a simple activation step followed by linear repolarization segments. Each point in the model was assigned an activation time from Durrer's measurements [28]. Despite the simplicity of the model, the electrocardiograms produced by the model for the normal activation were very well in line with measured data, i.e., normal body surface potential maps and electrocardiograms. In the second paper, Miller and Geselowitz created ischemic regions to the heart model by modifying the action potentials and assigning an activation delay to the elements in the ischemic region. Again, the results produced by the model were consistent with recorded data from patients with ischemic heart disease. Geselowitz and Miller later described the computation of body surface potentials and magnetic fields from the simulated cardiac sources [35, 34]. They provided some argumentation as to why the anisotropy of the cardiac muscle is not significant in computing the body surface potentials. We have found that the anisotropy is not essential, but neglecting it provides clear differences from normal electrocardiograms and magnetocardiograms (unpublished observations relating to Publication VI).

Pollard and Barr describe perhaps one of the first realistic models for the human conduction system [105, 106]. The model has been built using data recorded from the human heart to come up with the proper activation times and a geometrical mapping of data on the anatomy of the conduction system on the heart model. The simulations show that there is marked similarity to measured data in the activation pattern.

Lorange *et al.* describe a model constructed from anatomical data of a human heart, wherein the fibre structure was generated by nesting ellipsoids in the ventricular walls and assigning realistically rotating fibre orientation [78]. The model also featured a simplistic conduction system that was able to reproduce the initial activation sites by Durrer [28]. The body surface potentials were computed by embedding the individual dipole sources into an inhomogeneous torso model. A speciality of this method is the use of so-called thorax extension method, whereby the anisotropic skeletal muscle layer below the surface of the torso is replaced by a thicker isotropic tissue. This method was also adopted in this work and it improved the robustness of the surface potentials to small variations in activation. Lorange *et al.* and Xu *et al.* have successfully simulated normal electrocardiograms [78], electrocardiograms resulting from a conduction block [79] and ectopic beats [146]. All the results have been validated against clinical data.

Dubé *et al.* demonstrate the ability of their heart model to simulate ischemia [26]. They show

normal electrocardiograms and electrocardiograms from a heart with an occlusion in any of the major arteries. All results are in good agreement with literature data as well as measured data. With the theoretical model, they were able to show that the ST segment depression often visible on the other side of the heart than the occlusion is simply a result of the same ischemia, whereas earlier clinical reports had anticipated it to be a real physiological effect.

Berenfeld *et al.* describe a model based on the FitzHugh-Nagumo action potential model in a heart model with cubical lattice and a cell spacing of 1 mm [9]. The effect of the FitzHugh-Nagumo model parameters to the action potential shape and considerations on the effects of rotational anisotropy are presented. In the core of the model, they used regular three-by-three differentiation formulas, wherein the second cross derivatives are computed by using the four corner cells in the plane of the differentiation. The heart model is fairly coarse, with only 145,000 cells in the model. In the cardiac muscle, the propagation velocity was 1.2 m/s, but for the Purkinje fibers an artificial boost was added to get the propagation velocity to 2.5 m/s. As a result, Berenfeld *et al.* show a V5 lead in normal conditions and two different levels of ischemia. They claim that the V5 lead signal is similar to a real signal. It seems, however, that the model is not able to reproduce the end of the QRS complex accurately, as the negative S deflection is completely missing. This could indicate that the initial insertion sites of the Purkinje fibers that are well known are properly positioned, but the later sites or the fiber structure of the ventricles fail to mimick reality.

In a later publication [10], Berenfeld *et al.* have taken the conduction system information by Tawara [134] and applied it to their model which also incorporates the fibrous structure of a canine heart. They show all 12-lead electrocardiographic leads as well as the activation isochrones in three sections. Their electrocardiograms seem more normal than in their earlier work, but still fail to demonstrate a late activation towards the posterobasal wall in the left ventricle. They claim that the isochrones match with measured isochrones by Durrer [28], but there are at least two apparent differences. First, there is no area in the left ventricle that would be devoid of the conduction system. This may be because they adopted Tawara's information as such by scanning and superimposing his pictures on their heart model. Tawara claims to have seen the Purkinje system on the endocardium by naked eye, but later studies have shown that this is not possible for the distal Purkinje network. Moreover, Durrer's data clearly shows that there is no conduction system present in a CCW spiral-like zone from the apex to the base on the epicardium of the free wall of the left ventricle. Secondly, the wavefront propagation disagrees markedly with Durrer's measurements. There is no demonstration of intramural propagation in the direction of fibers as there is in Durrer's data, and the activation wave fronts go rather steadily from the endocardium to the epicardium. This may be because of the model characteristics, coarsity of the geometry or numerical effects. In fact, the authors even indicate that the Purkinje-myocardial junctions are treated differently to avoid numerical instability. Berenfeld *et al.* have simulated Purkinje-muscle re-entry, but in fact Ben Haim *et al.* found little evidence of the occurrence of such in experiments [7], although the geometric conditions of Purkinje-muscle junctions would probably favour this behaviour [89].

Huiskamp shows that a model with realistic fibre geometry applying the equal anisotropy ratios can reproduce true electrocardiograms reasonably well [59]. What is suprising is that with a fairly coarse stimulus network (four sites), good quality electrocardiograms are produced. This finding disagrees somewhat with our findings, where the shape of the conduction system was the determining factor of the electrocardiograms' goodness.

Winslow *et al.* describe the construction of a realistic heart model combining a state-of-the-art

cell model and anatomically accurate geometric model where fibre geometry has been obtained from diffusion tensor magnetic resonance imaging (DTMRI) [144]. Mäkelä *et al.* have been successfully applying modern anatomical imaging methods like deformable models for cardiac source imaging [84, 85]. Apart from source imaging, anatomical models obtained in this manner can be applied to model the cardiac activation individually. By using deformable models and accurate fibre geometry, both an individualized heart model and an individualized model of the thorax could be obtained.

Sermesant *et al.* describe a model where the mechanical contraction is coupled to the electrical activation [116]. The model uses a FitzHugh-Nagumo action potential model and a geometric model with 256 nodes. The exact activation pattern remains somewhat unclear, although the authors report good results in the mechanical contraction as compared to imaging data from the beating heart.

He *et al.* and Li *et al.* introduce the use of their anisotropic heart model for localizing the origin of cardiac activity [75], for carrying out activation time mapping [42] and for determining the transmembrane potential distribution in the heart [43]. The basic principle of this approach is to impose goodness-of-fit measures to the propagated activation and the simulated body surface potentials and to apply optimization to achieve the best match. The approach was validated with a single patient, wherein the localization accuracy was found to be of the order of 5 mm [76].

5.2 The Dalhousie propagation model

Horáček *et al.* and Nenonen *et al.* have previously presented the salient properties of the model used in this work [95, 96, 54, 97]. Both the anisotropic bidomain theory and the computer implementation of the model are described. Together with activation isochrones in a slab, the resulting electromagnetic fields are shown, in comparison with some measured data. It is stressed that the anisotropic properties are significant in the generation of extracardiac fields. For example, an intramural source would not generate any electric signal without the anisotropic component.

Leon *et al.* were able to observe directional differences in the current bidomain model that has equal anisotropy ratios for the intracellular and extracellular spaces [74]. Moreover, the model reproduces reasonably well the shape of the electrograms recorded by Witkowski [145]. Leon *et al.* also demonstrate the importance of the axial current component in the formation of body surface potential maps, whereas in earlier uniform double layer models this contribution does not exist (since the double layer is indeed uniform). In the present work, this contribution of the axial current component was found to be an essential feature for producing realistic body surface potential maps from simulated normal activation.

Hren *et al.*, using the fibre geometry and an earlier computation engine of the present model, were able to show that the simulated body surface potential maps computed from the propagated activation that resulted from the artificial pacing stimulus in various locations of the ventricles agree well with clinically recorded data [56, 125]. This demonstrates that the fiber structure of the model is macroscopically realistic and the propagated excitation most likely reproduces the true activation of the human heart in the case of catheter pacing. Furthermore, the results indicate that the methods for computing the body surface potentials produce realistic results. In another

paper, Hren *et al.* show that the same method can be used for localizing the accessory pathways in Wolff-Parkinson-White patients [58].

Hren *et al.*, again using the fibre geometry of the present model, were able to demonstrate the effect of fibre rotation through the wall of the cardiac muscle to have an effect on the epicardial potentials [57]. Similar effects as were seen in Hren's simulations were measured from the dog heart by Taccardi [132]. This demonstrates the validity of the computational model taking into account the fibre structure and also, again, the methods for computing the electromagnetic fields.

The propagation model consists of 2.000.000 excitable elements comprising the conduction system and the myocardium and 8.000.000 non-excitable elements making up the intra- and extracardiac volumes. The elements are located on a cubic lattice with 0.5-mm spacing. The geometry was reconstructed from photographic images of 1-mm frozen slices of the human heart. The assignment of the principal fiber direction was performed separately for left-ventricular, right-ventricular and papillary-muscle cells, with the fiber direction rotating from endocardium to epicardium [130].

Our hybrid model of the ventricular myocardium describes the subthreshold behaviour of the elements according to the anisotropic bidomain theory [20], while in the suprathreshold region the elements behave as cellular automata. The model consists of 2×10^6 excitable elements on a cubic lattice with 0.5-mm spacing [57]. Each element is assigned a specific *type* and a vector of local *fiber direction* [132]. During simulation, elements undergo a series of state transitions. Their electrotonic interactions are governed by the generalized cable equation (Eq. 21), which is derived under an assumption of equal anisotropy ratios [74, 95]. Physiological parameters for the model are adopted from literature [128, 105, 18, 111]. The development of the numerical propagation algorithms in this work are described in Publication V.

We computed the extracardiac fields as described in section 3.6, i.e., the anisotropy in the cardiac muscle was taken into account. Since it is difficult to determine the effect of anisotropy on the body surface potentials experimentally, we evaluated the effect of different levels of anisotropy on the BSPM computed from the simulated activation. To do this, we computed the body surface potential maps separately for the isotropic and the axial component of the source dipoles according to Eq. (32). Subsequently, we summed the two potential maps with a weighting. We found that the weighting of 2:1 of the isotropic and axial potential maps produced the most realistic BSPM sequence (Publication VI). This is consistent with the effect of the extracellular medium on body surface potentials suggested by Geselowitz: the more isotropic extracellular space should attenuate the effect of the intracellular anisotropy [35]. The nodes closest to corresponding ECG electrodes for the limb leads were used in the construction of the Wilson Central Terminal (WCT). The electrocardiograms and vectorcardiograms were then computed by using the nodes closest to corresponding ECG electrodes (see Fig. 7).

5.3 Conduction system model

In this work, we required the conduction system to produce correct body surface electromagnetic fields — the electrocardiograms and magnetocardiograms — and activation rather than to strictly follow any predetermined anatomical pattern. A computer program for the interactive editing of the conduction system was created with the OpenGL capabilities of the SGI Visual PC. The

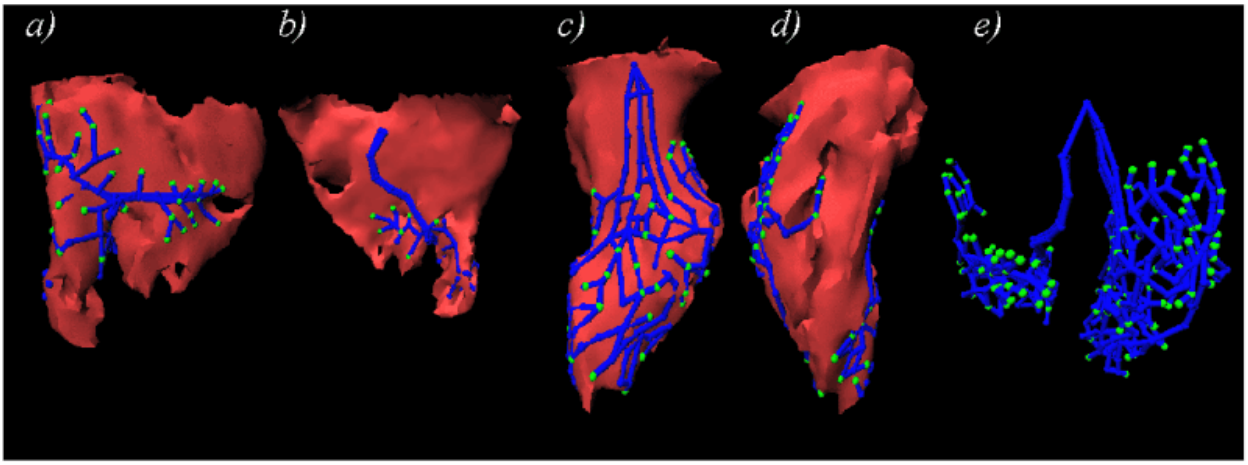

Figure 19: *The geometry of the conduction system observed from different angles. The right branch of the His bundle (not shown) connects the topmost nodes of the left and right conduction system. In the RV apical view (a), notice how the moderator band contains the conduction system activating the RV free wall and the papillary muscles (arrow). The RV free wall (b) and septal (c) views show the right conduction system, consisting of one main bundle with several smaller branches. The views of LV septum (d) and LV free wall (e) show the more complicated structure of the left conduction system. Notice the fan-like structure of the septal conduction system in (d), and the vertical spiral gap (dashed area) in the conduction system in (e). The PMJs are shown as light spheres.*

program requests the user to select a surface, on which the conduction system will be designed, and also allows some simple modifications of this surface. For this purpose, a triangulated surface of the intracavitary blood masses was created from the corresponding volumes of the ventricular model [80].

The user can create nodes on the surface, by pointing to the desired location, and connect these nodes, that is, define the connection matrix for the nodes. The nodes can later be repositioned, and the connection matrix can be modified. The nodes are automatically named to represent their location, but the names also reflect their functionality: some nodes are just connection points for the conduction system, while some are actual Purkinje–myocardial junction sites (PMJs), where the activation enters the myocardium.

The geometry of the conduction system is shown in Fig. 19. The His bundle consists of a single branch in the right ventricle, whereas it resembles a fan-like sheet of fibers in the left ventricle. The His bundle continues on both sides as the Purkinje network that contains the Purkinje-myocardial junction (PMJ) sites. On the right, the most prominent feature of the conduction system is the single bundle that carries the activation from the septum to the free wall and the papillary muscles along the moderator band. On the left, there are three major areas of activation: the septum and the inferior and superior free wall. There is no conduction network in the posterior free wall.

The volume model for simulations was created on a 1.5-mm thick endocardial layer by first projecting the nodes onto this layer and then tracing the connections. The thickness of the connections and PMJ sites was adjusted to ensure connectivity and proper propagation between the conduction system and the myocardium. By changing the conductivity properties, the propagation velocity was adjusted to approximately 2.0 m/s. The activation time of a PMJ site was completely defined

by the propagation through the conduction system. The volume model was superimposed on the model of the ventricular myocardium at the beginning of the simulation (see Publication VI).

5.4 Simulation of normal activation

More than 200 simulations were run to iteratively determine correct parameters for the anisotropic bidomain model, to create an anatomically correct conduction system, and to investigate the effects of geometry on the electromagnetic fields. First, a reasonable set of parameters were chosen for the initial analyses on the anatomy of the conduction system. Then, as the conduction system produced a good match with experimental invasive data, the parameters were fine-tuned to give correct QRS duration and timing for the breakthroughs. After this, initial modifications to the thorax geometry were made by comparing the location and orientation of the heart in the thorax model to anatomical textbooks and imaging data. Finally, after some adjustments to the conduction system, the geometry was finalized using the vectorcardiogram as a guide, still keeping the geometry within anatomically normal limits.

The simulations were run with a time step of 50 μs. Time steps between 5 μs and 100 μs all yielded consistent isochrones, and the value of 50 μs was chosen as a compromise between numerical accuracy and computation speed. With a time step of 50 μs, the 150 ms simulation of the QRS took 1,5 hours on a 650 Mhz Pentium III personal computer. Correct QRS duration was achieved by using surface-to-volume ratio of $\chi = 1200\mathrm{cm}^{-1}$ for the cardiac cell, axial conductivity $\sigma_l = 2.5$ mS/cm and transverse conductivity $\sigma_l = 0.5$ mS/cm.

The initial shape of the conduction system was built to match the anatomical descriptions presented earlier. Modifications were later made mostly to balance the timing of different directions of initial activation. This was achieved by adjusting the basal location of the His bundle, by changing the length of the right bundle branch by altering its course, and by modifications of the left bundle branches. The thickness of the fibers was also varied, as was the spatial extent of the Purkinje-myocardial junctions. With these modifications, we achieved a reasonable match with measured activation sequences of the human heart.

As the geometry of the ventricles was taken from a different subject (a victim of a traffic accident) than the geometry of the thorax (normal volunteer), the heart had to be refitted inside a thorax model manually. With a 3D-manipulator program, an experienced cardiologist determined a normal position and orientation of the heart within the thorax, which was then evaluated against anatomical textbooks, expert descriptions and cardiac imaging data.

The simulated activation sequence shown in Figure 21 agrees with isochrones obtained from an isolated human heart [28]. Additionally, the activation sequence during left bundle branch block was used for comparison in the right ventricle [21]. The ventricular activation starts in the left ventricular septum (layer 110), matched by a right ventricular septal activation 20 ms later (layers 70–90). Almost simultaneously with the RV septal activation, the inferior (in body coordinates) and anterior LV activation appear (layers 90–110). These are followed by the activation of the RV free wall (layers 90–130). The RV and LV breakthroughs take place at 30 ms and 45 ms, respectively. In the final stages of the QRS, activation propagates through the posterior LV free wall and the pulmonary conus.

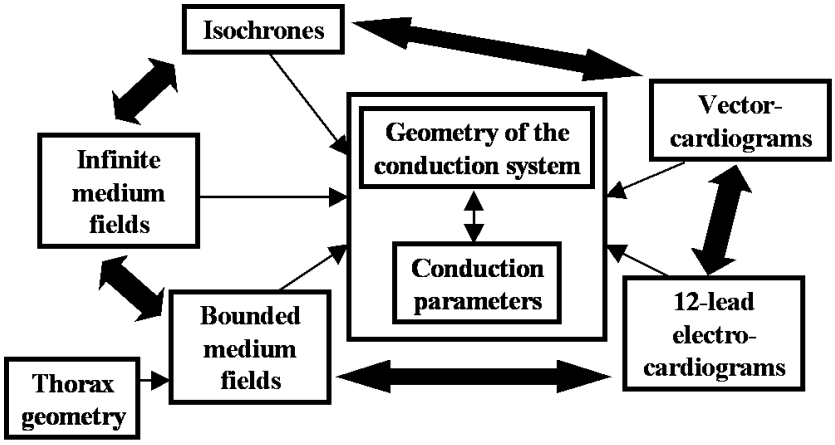

Figure 20: The process of adapting the conduction system model to produce proper exctracardiac fields. By modifying the geometry of the conduction system and by changing the conduction parameters, each of the modalities of the measurable activation is affected: the isochrones, infinite and bounded medium fields, the 12-lead electrocardiograms and the vectorcardiograms.

The calculated body surface potential maps during the initial QRS complex correlated well with our clinical recordings on normal subjects. However, the variation in normal BSPMs is significant due to, e.g., deviations in the individual activation sequence. Therefore, we selected here a BSPM sequence for comparison according to the description of normal activation by Selvester *et al.* [115].

Figure 22 shows simulated BSPMs during the initial QRS complex. The initial maximum resulting from left septal activation is anterior and slightly superior. Then, the minimum on the back moves upward and travels over the right shoulder onto the right anterosuperior region, indicating apical activation and masking of the left septal activation by the corresponding right septal activation. The area of positive potentials then drifts to the back, as the right ventricular breakthrough happens, and the activation in the left ventricle travels mainly to the posterior direction. Finally, a positive area appears in the high posterior area, resulting from the activation of the pulmonary conus.

We computed the magnetocardiographic maps on a planar surface above the chest. The sensors in the MCG recording are arranged similarly, which makes comparison easy. Due to the geometry, the MCG “sees" primarily the sources that are parallel to the frontal plane (see the vectorcardiogram below) [98]. The MCG is sensitive to activation wavefronts that are close to the sternum and moving in the frontal plane, whereas other currents (deeper and other directions) need to be much stronger to be picked up by the MCG to the same extent.

The simulated magnetocardiographic maps are shown in Fig. 23. The initial septal activation is not very well reflected on the MCG, but the apical activation is clearly visible as a bipolar field pattern pointing down and to the left by the right hand rule. The right ventricular brakthrough creates a “twist" to the field pattern, and late basal activation and the activation in the pulmonary conus are visible.

The time development of the surface potential at the locations of the 12-lead ECG is extensively documented, and the cardiac processes producing deviations to the temporal morphology are well understood. Moreover, the vectorcardiogram describes in great detail the electrical activation of the heart in relation to its 3-dimensional geometry [44]. These features of the standard clinical

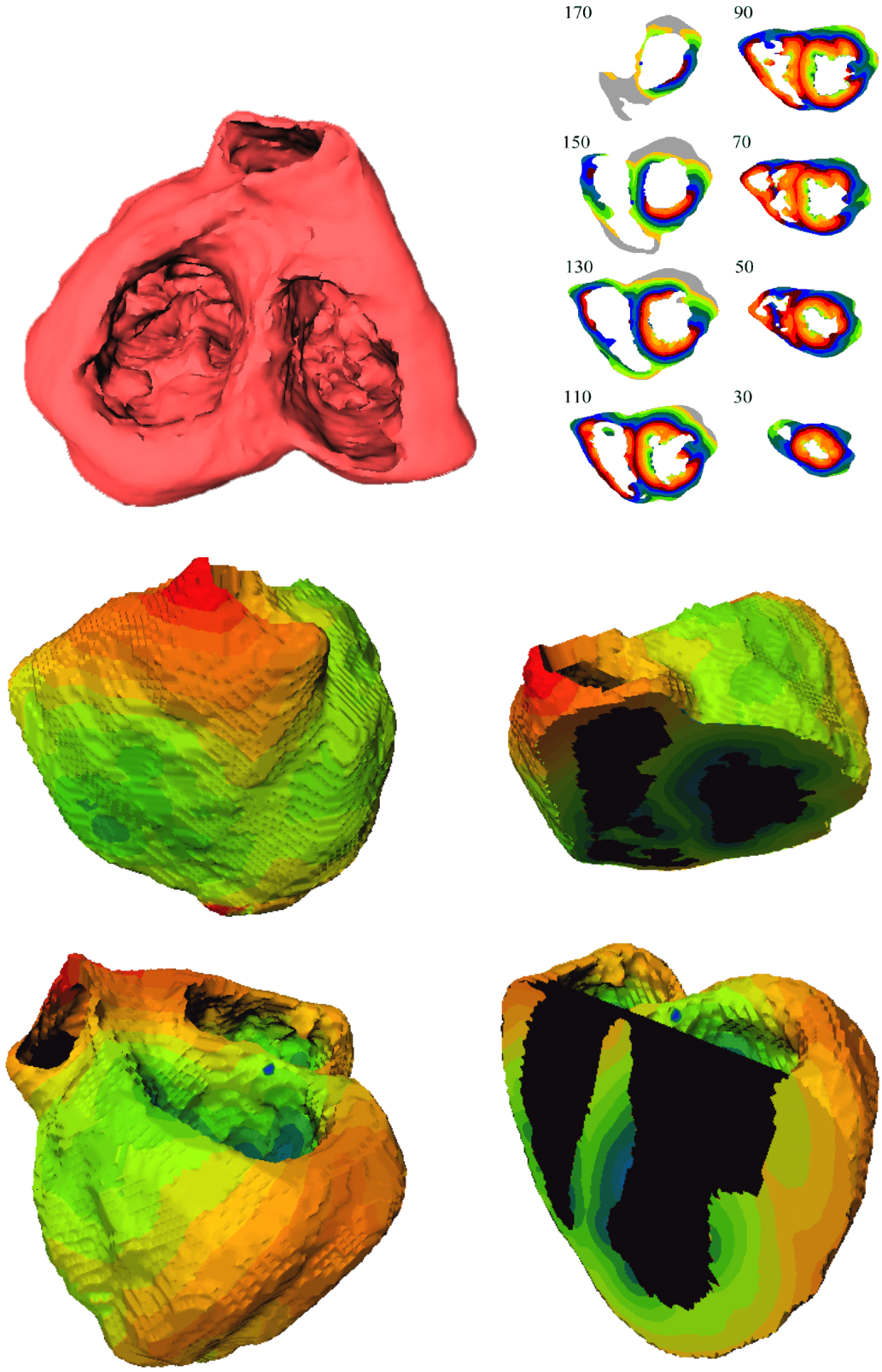

Figure 21: Isochrones of simulated normal activation of the ventricles. The top left panel shows a basal view of the ventricles, and the top right view displays the activation isochrones on layers that are parallel to the basal ring. The middle and bottom panels display different three-dimensional views of the activation.

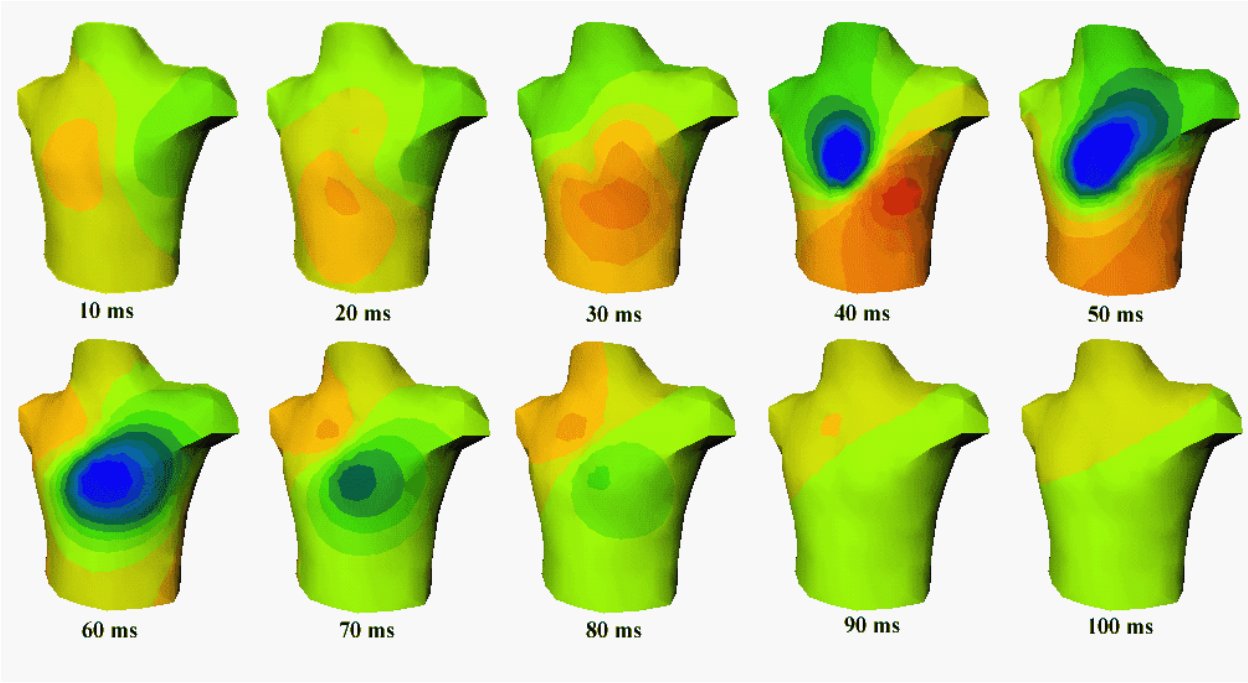

Figure 22: Simulated body surface potential maps during ventricular activation. In the computation of the simulated BSPMs, the effects of the thorax surface and the lungs have been taken into account [100]. The effect of anisotropic thorax muscle was modeled by the thorax extension method [26].

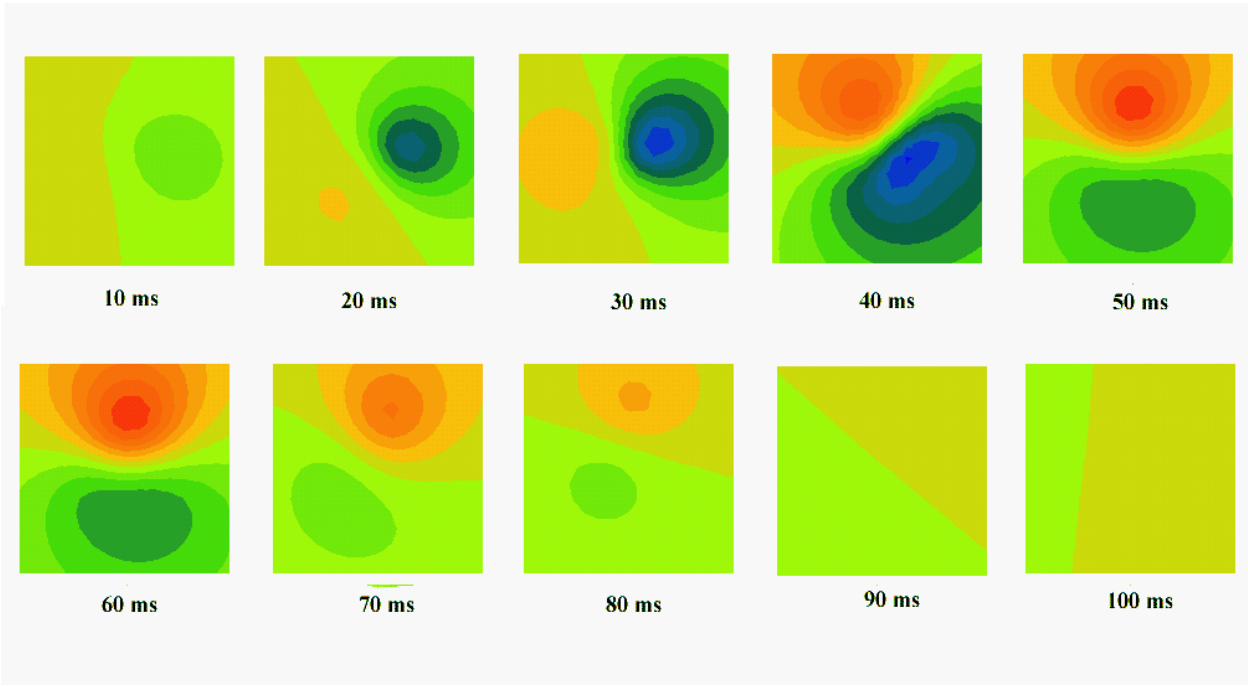

Figure 23: The z-component of simulated magnetocardiographic maps during ventricular activation. Blue indicates flux coming out of the chest and red indicates flux entering the chest. The effects of the thorax inhomogeneities (lungs and thorax surface) were taken into account as presented in [100].

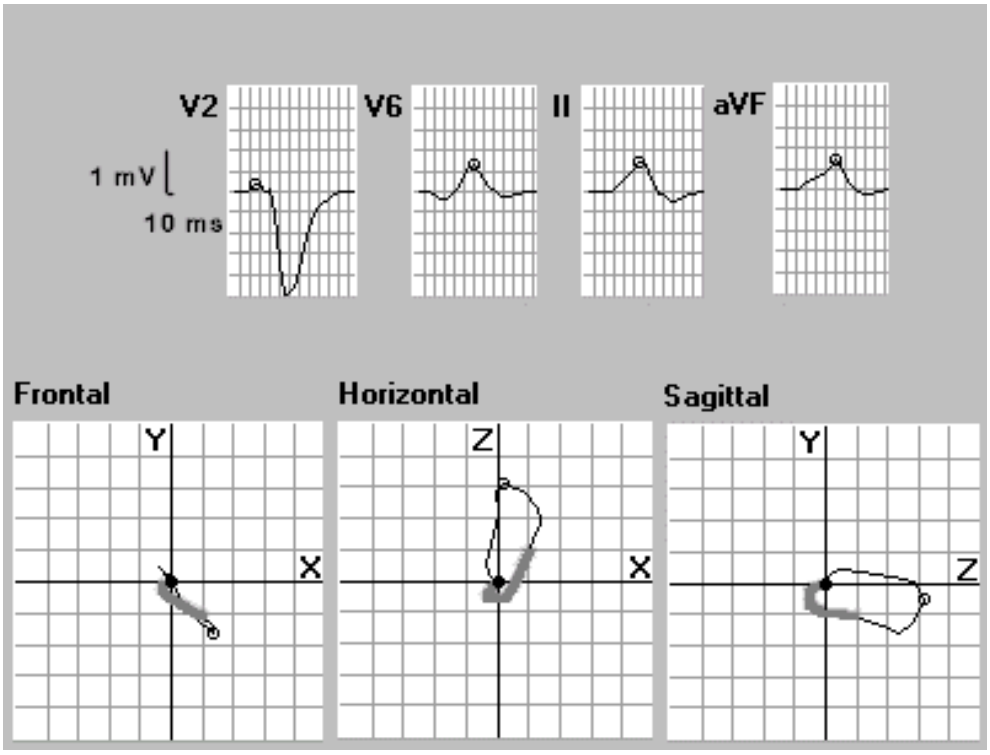

Figure 24: The limb leads II and aVF, the chest leads V2 and V6, and the horizontal, sagittal and frontal loops of the vectorcardiogram.

tools provide the strictest means to judge our ventricular model. The prominent features of the 12-lead electrocardiogram and the vectorcardiogram were indeed reproduced in the simulations (see Fig. 24). However, some smaller deviations from the normal electrocardiogram are still present in the modeled ECG, and these will be described in the discussion.

The signal morphology in the chest leads of the 12-lead electrocardiogram correctly shows an increase in the R wave amplitude from lead V1 to V6, and simultaneously a decrease in the S wave amplitude. The crossover from prominent S to prominent R morphology takes place between V4 and V5. The augmented limb leads show the following features: the aVR is mainly negative, and the aVF mainly positive, while the aVL has a slightly negative but very unclear morphology. The aVR displays abnormal late positivity. This is reflected to the leads I, II and III that are otherwise normal.

The vectorcardiogram shows a “tight" clockwise loop pointing to low right in the frontal plane: the frontal angle is $59.6°$. In the horizontal plane, the wide counterclockwise loop points mainly in the left posterior direction. The sagittal loop is counterclocwise and points to low posterior direction.

Information from anatomical and electrophysiological studies on the conduction system are to some extent contradictory. For example, bundle branch blocks are usually functional phenomena, where the anatomy of the conduction may be completely intact. Moreover, very different conduction system anatomies often produce similar normal ECGs. Therefore, it is important to differentiate between true anatomical defects and functional anomalies: the electrophysiologically meaningful concept of left hemiblocks often has no basis in anatomy, especially in the ischemic heart. The modelling is further complicated by the fact that anatomical information on the conduction system is old, and no digital data are available. Furthermore, few thorough works on activation

sequences of the human heart exist.

Several details used in our model algorithm are still under discussion in the scientific community. For example, it is still somewhat unclear, whether simplifying the modelling of anisotropic properties by the use of equal anisotropy ratios affects the propagation significantly. The effect of thoracic and cardiac muscle anisotropies on the forward solution has also been discussed. Our assumption in this paper is that anisotropy has little effect on activation, but may be important in the forward computation. However, more fundamental features like transmurally varying cell properties may mask the effects of anisotropy, especially in the repolarization phase. Therefore, the effect of action potential heterogeneity (M-cells) has to be studied further [2].

The activation sequence produced by our simulations was compared to the activation sequence measured from the isolated human heart [28]. The simulated activation of the left ventricle matched very well the recorded one, when the cross sections are aligned. However, the data from Durrer *et al.* almost totally lacks right septal activation, which is necessary to produce correct ECG. The trabecular muscles are problematic in segmentation, and our heart model features somewhat thicker inferior wall, and the inferior activation takes slightly too long. Also, the rigor mortis had probably set in at the time when the model was inflated to working cardiac pressure, which makes the ventricular walls appear thicker than in the living state.

The simulated body surface potential pattern corresponds to our recorded BSPMs with the exception of two features: the initial positive area on the anterior chest moves slightly too quickly to the back and the late activation (positive) of the pulmonary conus is too strong on the anterior chest. Both these features may be attributed to inaccurate positioning of the ventricular model within the thorax. The MCG transition corresponding to right ventricular breakthrough takes place in a different manner than in our recorded data, which may be due to neglecting the anisotropic properties of the thorax. Otherwise, the magnetocardiographic maps are consistent with recorded data.

The general outline on the simulated 12-lead ECG is normal. However, corresponding to the deviation in the BSPM, the 12-lead ECG also appears “rotated" to the left, and the crossover in chest lead morphology takes place between V4 and V5, not between V3 and V4 as usually. The strong pulmonary activation is reflected as an abnormal late positivity in the aVR lead. The vectorcardiogram is completely in the normal limits, the frontal angle being close to 60°, although the horizontal loop is also oriented sligthly too posteriorly.

Despite the simplifications in the model algorithm, our simulations produced correct activation sequence and “healthy" electro- and magnetocardiograms. Due to the lack of anatomical information of the Purkinje network, the anatomy of the conduction system was not restricted during the iterations. The final conduction system was, however, consistent with the literature on the anatomy. The conduction system was also robust, because small changes in the shape of the conduction system produced only unnoticeable or small effects on the electrocardiograms.

6 Discussion

Body surface potential mapping has perhaps long been viewed as a peculiar research tool with limited clinical utility. It is true that the distinct physical characteristics of the method — like the number of electrodes — are always going to be a factor limiting the clinical use of the method. However, other factors like the size and portability of the recording devices and the processing power required to analyze the signals are already mostly solved. In fact, it seems that the next challenge will be to develop suitable automated analysis methods for fast clinical application of body surface potential mapping, since there are already several common cardiac disorders where the method has proven its diagnostic power. Such analysis methods have also been introduced in this work (see Publications I to IV).

The traditional methods for risk assesment and localization of the source of cardiac arrhythmias have been extended in this work to multichannel electrocardiographic data. Publications III and IV display the application of the methods to patient studies. In Publication IV, it was found that the capability of body surface potential mapping to detect vulnerability to cardiac arrhythmias after a myocardial infarction was at least at the same level as that of the traditional signal-averaged electrocardiogram. It would be reasonable to assume that as new analysis methods are developed that utilize the superior spatial information present in body surface potential maps compared to traditional ECG instead of only extending the traditional ECG analysis methods, the ability of BSPM to identify patients at risk will be improved. For example, the mere addition of posterior leads in the recordings of Publication IV could improve the sensitivity to posterior arrhythmogenic sources. Methods like those in Publication I may also offer ways to fully utilize the spatial information in body surface potential mapping. In localization applications it may be important to take the temporal information into account to regularize the solutions. Earlier, it has not been easy to combine the spatial and temporal information of BSPM in one analysis method. It seems, therefore, that there is still much to be discovered in the use of BSPM data in clinical diagnosis.

Modelling cardiac electrical activity with realistic models shows a lot of potential for understanding the genesis of cardiac disorders like arrhythmias and ischemia and even in diagnosis of such disorders. Currently, there exist accurate models for the cardiac action potential, the cardiac tissue, the activation in the whole heart and the thorax as a volume conductor. However, combining the accuracy of these models is currently computationally too formidable a task, at least in a clinical setting, and simplifications have to be made when the cell-to-surface modelling chain is considered. Yet, it seems that the most significant factors affecting the modelling can be incorporated. Of course, the inclusion of details depends on the research question to which one is seeking an answer, i.e., whether the viewpoint is microscopic (cellular) or macroscopic (body surface potential and magnetic field).

This work focused on the modelling of cardiac depolarization in the normal heart. In fact, this task is more difficult than modelling the abnormal activation, e.g., during cardiac arrhythmias, since an accurate model of the conduction system has to be implemented. We were able to show that a model incorporating a proper computational engine on the cellular level (Publication V), tissue anisotropy due to fibre direction, anatomical structures like the conduction system (Publication VI) and a volume conductor model, is able to simulate the normal electrocardigram well. This work should now be extended by incorporating a more accurate action potential model, the contribution of the atria, and a proper model for ischemia. After such extensions, the model could be used to

studying the effect of drugs *in silico*, diagnosing ischemia, and even monitoring the efficacy of stem cell treatment.

Development of multimodal imaging is a prerequisite for the success of cardiac modelling. In the future, not only static anatomical data but also data on movement, fibre direction, perfusion and activation time need to be combined to yield a realistic model for the patient being examined. For this purpose, deformable models to match the individual anatomy, advanced magnetic resonance imaging to reveal the fibre structure and perfusion, and invasive methods or eletromagnetic source imaging to measure the activation time have been proposed. Even modelling the individual conduction systems may one day become possible. However, clinical application of individual modelling of cardiac activation will still require substantial research effort.

Reviewing the works of this thesis, it appears that the methods that have been presented create a path from traditional clinical analysis of the electrocardiogram — like the 12-lead ECG — to advanced modelling of the human heart. Publication II introduces a method that can be applied to both traditional electrocardiographic recordings as well as body surface potential mapping, while the need for the method is more apparent for clinical application of BSPM. Publication I presents a novel method utilizing the spatial characteristics and the large amount of information only provided by body surface potential mapping. Together, publications I and II introduce some advanced signal processing methods that are needed to take advantage of the multichannel body surface potential mapping data and magnetocardiographic data. Publication III provides an overview of the traditional and novel analysis methods applied to various recording methods, while publication IV evaluates the clinical utility of different recording and analysis methods in arrhythmia risk assessment. Publications III and IV demonstrate the viability of body surface potential mapping as a clinical tool. Finally, the modelling works of this thesis in publications V and VI utilized body surface potential mapping to validate the propagation model of the heart and the anatomical model of the thorax that were applied to simulation of normal cardiac activation.

It is envisioned that in the future it will be possible to implement the recording, analysis and modelling methods presented in this thesis on a portable device that could be carried with the person at all times. Such devices are already available to the public: mobile communication terminals — or cellular phones — possess significant processing and storage capabilities that in fact surpass that of personal computers 10 years ago. Each person could carry a model of his/her body and organs in the device, and by monitoring biological signals from the body, the models could be kept up to date in describing the current state of the different organs. For example, fairly common arrhythmias and ischemia could be monitored on-line by measuring the ECG at a couple of leads — perhaps subcutaneous wireless ECG leads — and simulating the condition that reproduces the measured signals.

It may be that the use of personal cardiac modelling will one day be as common as talking on the cellular phone is now.

Summary of publications

Publication I

K. Simelius, M. Stenroos, L. Reinhardt, J. Nenonen, I. Tierala, M. Mäkijärvi, L. Toivonen and T. Katila. Spatiotemporal characterization of paced cardiac activation with body surface potential mapping and self-organizing maps. *Physiol. Meas.* **24**, 805–816, 2003.

Application of body surface potential mapping (BSPM) to localization of arrhythmia sources in a clinical environment is demonstrated. The method is applied to patients suffering from ventricular tachyarrhythmias, and the localization is carried out by the use of self-organizing maps. The method was proven to be well suited for the analysis for the classification of the high-dimensional spatiotemporal data generated from BSPM during catheterization.

Publication II

T. Jokiniemi, K. Simelius, J. Nenonen, I. Tierala, L. Toivonen and T. Katila. Baseline reconstruction for localization of rapid ventricular tachycardia from body surface potential maps. *Physiol. Meas.* **24**, pp. 641–651, 2003.

In a rapid ventricular tachycardia, there is constantly an activation or repolarization process going on in the heart, which manifests itself on the body surface potential maps as constant electrical activity. As the QRS complex of the following beat overlaps the T wave of the preceding beat, a reliable baseline is difficult to establish. The method utilizes the variability in the beat-to-beat interval to reconstruct the underlying end of the T wave in order to obtain a clean QRS complex from the rapid tachycardia signal. The method showed good results when applied to noisy data.

Publication III

H. Väänänen, P. Korhonen, J. Montonen, M. Mäkijärvi, J. Nenonen, L. Oikarinen, K. Simelius, L. Toivonen and T. Katila. Non-invasive arrhythmia risk evaluation in clinical environment. *Herzschrittmachertherapie & Elektrophysiologie* **11**, 229–234, 2000.

Multichannel magnetocardiography and body surface potential mapping are applied to charaterization of the risk of life-threatening arrhythmias. The paper presents signal processing methods used for preprocessing the data, as well as those used to extract the parameters indicative of the risk: late fields and potentials, spectral variability, signal fragmentation and heart rate variability.

Publication IV

P. Korhonen, I. Tierala, K. Simelius, H. Väänänen, M. Mäkijärvi, J. Nenonen, T. Katila and L. Toivonen. Late QRS activity in signal-averaged magnetocardiography, body surface potential mapping, and orthogonal ECG in postinfarction ventricular tachycardia patients. *Ann. Noninvasive Electrocardiol.* **7**, 389–398, 2002.

Three methods for the evaluation of the propensity to life-threatening arrhythmias in postinfarction patients were compared: multichannel magnetocardiography (MCG), body surface potential

mapping (BSPM) and orthogonal three-lead signal-averaged electrocardiography (SAECG). The parameters provided by MCG and BSPM were found to be highly correlated, whereas the SAECG was found to be less correlated to the two others, and may therefore provide complementary information. The performance of MCG and BSPM was found to be similar or better than that of SAECG in identification of patients prone to arrhythmias.

Publication V

K. Simelius, J. Nenonen, V. Mäntynen, J.C. Clements and B.M. Horáček. A Hybrid Model of Cardiac Electrical Conduction. *Helsinki University of Technology Report TKK-F-A829*, 2004.

A model of the discretized myocardium based on bidomain equations is described, wherein the elements are allowed a comparatively large size. The inaccuracies from the large unit element size and from the computation of the second derivatives of the membrane potential are mitigated by introducing the concept of the bulk factor to the finite-size approximation and by transforming the Laplacian of the source term to a divergence. Together, these modifications allow a more accurate and speedy implementation of the model of a discretized myocardium on a single computer.

Publication VI

K. Simelius, J. Nenonen and B.M. Horáček. Modeling cardiac ventricular activation. *International J. on Bioelectromagnetism* **3**, pp. 51–58, 2001.

The electromagnetic fields created by the electrical activation of the heart are computed from excitation of a discretized model of the human ventricles through a model of the human conduction system imposed on the model. The membrane potentials of the elements of the model are used to compute the electrical dipoles present in the heart throughout the activation, and the extracardiac fields are evaluated from these dipoles by positioning the heart inside an inhomogeneous model of the thorax. The prominent characteristics of an average, measured body surface potentials and magnetocardiographic maps were reproduced by the model.

Author's contribution

The author was responsible in establishing the technical aspects of the clinical practice of body surface potential mapping in Publication I, and wrote most of the text. The author also wrote the software used in recording the BSPM data and analysing the recorded data on a personal computer according to the first method in the publication, and the analysis was carried out together with I. Tierala. The author invented the use of self-organizing maps on BSPM data, and assisted in the creation of the analysis software. In publication II, the first two authors developed and described the method together, while the first author wrote the software implementing the method. In publication III, the author was partially responsible for developing the program used in signal averaging, and invented the "tube" method presented in Fig. 1. In publication IV, the author contributed to the technical setup of the body surface potential mapping procedure. Publication V presents the improvements to the earlier discretized model of the myocardium introduced by the author, and was mostly written by the author. Publication VI presents the work by the author in modelling the conduction system of the human heart and the simulation results from the simulation runs carried out by the author. The last publication was completely written by the author.

References

[1] J. Abildskov. Electrocardiographic wave form and cardiac arrhythmias. *Am J Cardiol*, 64(2):29C–31C, 1989.

[2] C. Antzelevitch, S. Sicouri, S. Litovsky, A. Lukas, S. Krishnan, J. D. Diego, G. Gintant, and D.-W. Liu. Heterogeneity within the ventricular wall: Electrophysiology and pharmacology of epicardial, endocardial, and m cells. *Circ Res*, 69(6):1427–1449, 1991.

[3] A. Barnard, I. Duck, M. Lynn, and W. Timlake. The application of electromagnetic theory in electrocardiology. II. Numerical solution of the integral equations. *Biophys J*, 7:463–490, 1967.

[4] R. Barr and R. Plonsey. Field stimulation of 2-d sheets of excitable tissue. *IEEE Trans Biomed Eng*, 51:539–540, 2004.

[5] G. Baule and R. McFee. Detection of the magnetic field of the heart. *Am Heart J*, 66:95–96, 1963.

[6] G. Beeler and H. Reuter. Reconstruction of the action potential of ventricular myocardial fibres. *J Physiol*, 268:177–210, 1977.

[7] S. Ben-Haim, D. Cable, T. Rath, L. Carmen, and J. Martins. Impulse propagation in the Purkinje system and myocardium of intact dogs. *Am J Physiol*, 265:H1588–H1595, 1993.

[8] D. Benson, Jr., R. Sterba, J. Gallagher, A. W. II, and M. Spach. Localization of the site of ventricular preexcitation with body surface maps in patients with Wolff-Parkinson-White syndrome. *Circulation*, 65:1259–1268, 1982.

[9] O. Berenfeld and S. Abboud. Simulation of cardiac activity and the ecg using a heart model with a reaction-diffusion action potential. *Medical Engineering and Physics*, 18:615–625, 1996.

[10] O. Berenfeld and J. Jalife. Purkinje-muscle reentry as a mechanism of polymorphic ventricular arrhythmias in a 3-dimensional model of the ventricles. *Circ Res*, 82:1063–1077, 1998.

[11] C. Bradley, A. Pullan, and P. Hunter. Effects of material properties and geometry on electrocardiographic forward simulations. *Ann Biomed Eng*, 28:721–741, 2000.

[12] J. Braun and M. Sambridge. A numerical method for solving partial differential equations on highly irregular evolving grids. *Nature*, 376:655–660, 1995.

[13] H. Calkins, J. Langberg, J. Sousa, and et al. Radiofrequency catheter ablation of accessory atrioventricular connections in 250 patients: Abbreviated therapeutic approach in Wolff-Parkinson-White syndrome. *Circulation*, 85:1337–1346, 1992.

[14] E. Carmeliet. Mechanisms and control of repolarization. *Eur Heart J*, 98(Supp H):3–13, 1993.

[15] M. Cerqueira, N. Weissman, V. Dilsizian, A. Jacobs, S. Kaul, W. Laskey, D. Pennell, J. Rumberger, T. Ryan, and M. Verani. Standardized myocardial segmentation and nomenclature for tomographic imaging of the heart. *Circulation*, 105:539–542, 2002.

[16] R. Clayton. Computational models of normal and abnormal action potential propagation in cardiac tissue: linking experimental and clinical cardiology. *Physiol Meas*, 22:R15–R34, 2001.

[17] P. Colli Franzone, L. Guerri, and B. Taccardi. Potential distributions generated by point stimulation in a myocardial volume: Simulation studies in a model of anisotropic ventricular muscle. *J Cardiovasc Electrophysiol*, 4:438–458, 1993.

[18] P. Colli Franzone, L. Guerri, and B. Taccardi. Spread of excitation in a myocardial volume: Simulation studies in a model of anisotropic ventricular muscle activated by point stimulation. *J Cardiovasc Electrophysiol*, 4:144–160, 1993.

[19] P. Colli Franzone, L. Guerri, and S. Tentoni. Mathematical modelling of the excitation process in myocardial tissue: Influence of fiber rotation on wavefront propagation and potential field. *Math Biosci*, 101:155–235, 1990.

[20] P. Colli Franzone, L. Guerri, and C. Viganotti. Oblique dipole layer potentials applied to electrocardiology. *J Math Biol*, 17:93–124, 1983.

[21] R. Dam. Ventricular activation in human and canine bundle branch block. In H. Wellens, K. Lie, and M. Janse, eds., *The Conduction System of the Heart: Structure, Function and Clinical Implications*, pp. 377–392. Lea & Febiger, Philadelphia, 1976.

[22] R. Dam and M. Janse. Activation of the heart. In P. MacFarlane and T. Lawrie, eds., *Comprehensive Electrocardiology*, pp. 101–127. Pergamon Press, New York, 1989.

[23] J. Demoulin and H. Kulbertus. Histopathological examination of the concept of left hemiblock. *Brit Heart J*, 34:807–814, 1972.

[24] J. Demoulin and H. Kulbertus. Histopathological correlates of left posterior fascicular block. *Am J Cardiol*, 44:1083–1088, 1979.

[25] J. Demoulin and H. Kulbertus. Pathological correlates of intraventricular conduction disturbances. In A. Masoni and P. Alboni, eds., *Cardiac Electrophysiology Today*. Academic Press, 1982.

[26] B. Dubé, R. Gulrajani, M. Lorange, A. LeBlanc, J. Nasmith, and R. Nadeau. A computer heart model incorporating anisotropic propagation. IV. simulation of regional myocardial ischemia. *J Electrocardiol*, 29:91–103, 1996.

[27] M. Dubuc, R. Nadeau, G. Tremblay, T. Kus, F. Molin, and P. Savard. Pace mapping using body surface potential maps to guide catheter ablation of accessory pathways in patients with Wolff-Parkinson-White syndrome. *Circulation*, 87:135–143, 1993.

[28] D. Durrer, R. van Dam, G. Freud, M. Janse, F. Meijler, and R. Arzbaecher. Total excitation of the isolated human heart. *Circulation*, 41:899–912, 1970.

[29] W. Einthoven. Über die Richtung und die Manifeste Grösse der Potentialschwankungen im menschlichen Herzen und über des Einflus der Herzlage auf die Form des Elektrokardiogramms. *Pflügers Arch*, 150:275–315, 1913.

[30] G. Feld. Catheter ablation for the treatment of atrial tachycardia. *Progress in Cardiovascular Disease*, 36:205–224, 1995.

[31] P. Ganz and E. Braunwald. Coronary blood flow and myocardial ischemia. In E. Braunwald, ed., *Heart Disease — A Textbook of Cardiovascular Medicine*, pp. 1161–1183. W.B. Saunders Company, Philadelphia, 1997.

[32] M. Gardner, T. Montague, C. Armstrong, B. Horáček, and E. Smith. Vulnerability to ventricular arrhythmia: Assessment by mapping of body surface potential. *Circulation*, 73:684–692, 1986.

[33] Gaskell. On the innervation of the heart, with especial reference to the heart of the tortois. *J Physiol*, p. 43, 1883.

[34] D. Geselowitz. Description of cardiac sources in anisotropic cardiac muscle. application of bidomain model. *J Electrocardiol*, 25:Suppl:65–67, 1992.

[35] D. Geselowitz and W. Miller III. A bidomain model for anisotropic cardiac muscle. *Ann Biomed Eng*, 11:191–206, 1983.

[36] C. Giorgi, R. Nadeau, P. Savard, M. Shenasa, P. Pagé, and R. Cardinal. Body surface isopotential mapping of the entire QRST complex in the Wolff-Parkinson-White syndrome: Correlation with the location of the accessory pathway. *Am Heart J*, 121:1445–1453, 1991.

[37] D. Goldman. Potential, impedance, and rectification in membranes. *J Gen Physiol*, 27:37–60, 1943.

[38] M. Hämäläinen and J. Nenonen. Magnetic source imaging. In P. Lee, ed., *Engineering Superconductivity*, pp. 464–479. Wiley-Interscience, New York, 2001.

[39] H. Hänninen, P. Takala, M. Mäkijärvi, P. Korhonen, L. Oikarinen, K. Simelius, J. Nenonen, T. Katila, and L. Toivonen. ST-segment level and slope in exercise-induced myocardial ischemia evaluated with body surface potential mapping. *Am J Cardiol*, 88:1152–1156, 2001.

[40] H. Hänninen, P. Takala, J. Rantonen, M. Mäkijärvi, K. Virtanen, J. Nenonen, T. Katila, and L. Toivonen. ST-T integral and T-wave amplitude in detection of exercise-induced myocardial ischemia evaluated with body surface potential mapping. *J Electrocardiol*, 36:89–98, 2004.

[41] D. Harrild, R. Penland, and C. Henriquez. A flexible method for simulating cardiac conduction in three-dimensional complex geometries. *J Electrocardiol*, 33:241–251, 2000.

[42] B. He, G. Li, and X. Zhang. Noninvasive three-dimensional activation time imaging of ventricular excitation by means of a heart-excitation model. *Phys Med Biol*, 47:4063–4078, 2002.

[43] B. He, G. Li, and X. Zhang. Noninvasive imaging of cardiac transmembrane potentials within three-dimensional myocardium by means of a realistic geometry anisotropic heart model. *IEEE Trans Biomed Eng*, 50:1190–1202, 2003.

[44] J. Heikkilä. *EKG, perusteet ja tulkinta*. Lääketehdas Orion, 2nd edn., 1991.

[45] C. Henriquez. Simulating the electrical behavior of cardiac tissue using the bidomain model. *CRC Crit Rev Biomed Eng*, 21:1–77, 1993.

[46] C. Henriquez, A. Muzikant, and C. Smoak. Anisotropy, fiber curvature and bath loading effects on activation in thin and thick cardiac tissue preparations: Simulations in a three-dimensional bidomain model. *J Cardiovasc Electrophysiol*, 7:424–444, 1996.

[47] B. Hille. *Ionic Channels of Excitable Membranes*. Sinauer Associates Inc., Sunderland, Massachusetts, 2nd edn., 1992.

[48] W. His. Die Tätigkeit des embryonalen Herzens und deren Bedeutung für die Lehre von der Herzbewegung beim Erwachsenen. *Arbeiten aus der med. Klinik zu Leipzig*, pp. 14–49, 1893.

[49] A. Hodgkin and B. Katz. The effect of sodium ions on the electrical activity of the giant axon of the squid. *J Physiol (London)*, 108:37–77, 1949.

[50] P. Holt, C. Smallpiece, P. Deverall, and *et al*. Ventricular arrhythmias, a guide to their localization. *British Heart Journal*, 53:417–430, 1985.

[51] B. Horáček. Digital model for studies in magnetocardiography. *IEEE Trans Magn*, MAG-9:440–444, 1973.

[52] B. Horáček and J. Clements. The inverse problem of electrocardiography: A solution in terms of single- and double-layer sources on the epicardial surface. *Mathematical Biosciences*, 144(2):119–154, 1997.

[53] B. Horáček, W. Eifler, H. Gewirtz, R. Helppi, P. Macaulay, J. Sherwood, E. Smith, J. Tiberghien, and P. Rautaharju. An automated system for body-surface potential mapping. In H. Ostrow and K. Ripley, eds., *Computers in Cardiology*, pp. 399–407. IEEE Computer Soc., Long Beach, CA, 1977.

[54] B. Horáček, J. Nenonen, J. Edens, and L. Leon. A hybrid model of propagated excitation in the ventricular myocardium. In D. Ghista, ed., *Biomedical and Life Physics*, pp. 181–190. Vieweg Verlag, Wiesbaden, 1996.

[55] B. Horáček, E. Smith, D. Cameron, H. Gewirtz, and P. Rautaharju. Iso-integral analysis of body surface potential maps. In P. Macfarlane, ed., *Progress in electrocardiology*, pp. 22–27. Pitman Medical, Kent, 1979.

[56] R. Hren and B. Horáček. Value of simulated body surface potential maps as templates in localizing sites of ectopic activation for radiofrequency ablation. *Physiol Meas*, 18:373–400, 1997.

[57] R. Hren, J. Nenonen, and B. Horáček. Simulated epicardial potential maps during paced activation reflect myocardial fibrous structure. *Ann Biomed Eng*, 26:1–14, 1998.

[58] R. Hren, G. Stroink, and B. Horáček. Localization of septal accessory pathways in WPW syndrome using simulated body surface potential maps as templates. In A. Murray and S. Swiryn, eds., *Computers in Cardiology*, pp. 21–24. IEEE Computer Society Press, Piscataway, NJ, 1997.

[59] G. Huiskamp. Simulation of depolarization in a membrane-equations-based model of the anisotropic ventricle. *IEEE Trans BME*, 45:847–855, 1998.

[60] J. Jack, D. Noble, and R. Tsien. *Electric Current Flow in Excitable Cells*. Clarendon Press, Oxford, 1983.

[61] J. Jalife and J. Davidenko. Spiral waves as a mechanism of reentrant excitation in isolated cardiac muscle. In M. Shenasa, M. Borggrefe, and G. Breithardt, eds., *Cardiac Mapping*, pp. 607–623. Futura Publishing, Mount Kisco, NY, 1993.

[62] M. Jazayeri. Atrioventricular nodal reentrant tachycardia: Characterization of the reentrant circuit before and after selective fast or slow pathway ablation. In M. Shenasa, M. Borggrefe, and G. Breithardt, eds., *Cardiac Mapping*, pp. 411–434. Futura Publishing, Mount Kisco, NY, 1993.

[63] M. Josephson, A. Harken, and L. Horowitz. Long-term results of endocardial resection for sustained ventricular tachycardia in coronary disease patients. *Am Heart J*, 104:51–7, 1982.

[64] M. Josephson, L. Horowitz, and H. Waxman. Sustained ventricular tachycardia: Role of the 12-lead electrocardiogram in localizing site of origin. *Circulation*, 64:257–272, 1981.

[65] M. Josephson, H. Waxman, M. Cain, M. Gardner, and A. Buxton. Ventricular activation during ventricular endocardial pacing. II. Role of pace-mapping to localize origin of ventricular tachycardia. *Am J Cardiol*, 50:11–22, 1982.

[66] R. Kaaja. *Muscular fibre architecture of the left ventricular wall in normal and hypertrophied rat hearts: Application of the plastic injection method*. Ph.D. thesis, University of Helsinki, Finland, 1984.

[67] S. Kamakura, N. Aihara, M. Matsuhisa, T. Ohe, and K. Shimomura. The role of initial minimum potentials on body surface maps in localizing the earliest endocardial site of ectopic vetricular excitation (abstract). *Circulation*, 74(Suppl II):II–138, 1986.

[68] A. Katz. *Physiology of the Heart*. Lippincott Williams & Wilkins, 3rd edn., 2000.

[69] J. Kemmelings, A. Linnenbank, S. Muilwijk, A. SippensGroenewegen, A. Peper, and C. Grimbergen. Automatic QRS onset and offset detection for body surface QRS integral mapping of ventricular tachycardia. *IEEE Trans Biomed Eng*, 41:830–836, 1994.

[70] D. Klug, A. Ferracci, F. Molin, M. Dubuc, P. Savard, T. Kus, F. Hélie, R. Cardinal, and R. Nadeau. Body surface potential distributions during idiopathic ventricular tachycardia. *Circulation*, 91:2002–2009, 1995.

[71] T. Kohonen. *Self-Organizing Maps*. Springer-Verlag, Berlin, 1995.

[72] T. Kohonen, J. Hynninen, J. Kangas, J. Laaksonen, and K. Torkkola. *LVQ-PAK, The Learning Vector Quantization program package*. Helsinki University of Technology, Laboratory of Computer and Information Science, 1995.

[73] D. Kuchar, J. Ruskin, and H. Garan. Electrocardiographic localization of the site of origin of ventricular tachycardia in patients with prior myocardial infarction. *J Am Coll Cardiol*, 13:893–900, 1989.

[74] L. Leon and B. Horáček. Computer model of excitation and recovery in the anisotropic myocardium. *J Electrocardiol*, 24:1–41, 1991.

[75] G. Li and B. He. Localization of the site of origin of cardiac activation by means of a heart-model-based electrocardiographic imaging approach. *IEEE Trans Biomed Eng*, 48:660–669, 2001.

[76] G. Li, X. Zhang, J. Lian, and B. He. Noninvasive localization of the site of origin of paced cardiac activation in human by means of a 3-D heart model. *IEEE Trans Biomed Eng*, 50:1117–1120, 2003.

[77] J. Liebman, J. Zeno, B. Olshansky, A. Geha, C. Thomas, Y. Rudy, R. Henthorn, M. Cohen, and A. Waldo. Electrocardiographic body surface potential mapping in the Wolff-Parkinson-White syndrome: Noninvasive determination of the ventricular insertion sites of accessory atrioventricular connections. *Circulation*, 83:886–901, 1991.

[78] M. Lorange and R. Gulrajani. A computer heart model incorporating anisotropic propagation. I. Model construction and simulation of normal activation. *J Electrocardiol*, 26:245–261, 1993.

[79] M. Lorange, R. Gulrajani, R. Nadeau, and I. Préda. A computer heart model incorporating anisotropic propagation. II. simulations of conduction block. *J Electrocardiol*, 26:263–277, 1993.

[80] J. Lötjönen, P.-J. Reissman, I. Magnin, J. Nenonen, and T. Katila. A triangulation method of an arbitrary point set for biomagnetic problems. *IEEE Trans Magn*, 34(4):2228–2233, 1998.

[81] C.-H. Luo and Y. Rudy. A dynamic model of the cardiac ventricular action potential. I. Simulations of ionic currents and concentration changes. *Circ Res*, 74:1071–1096, 1994.

[82] M. Lynn and W. Timlake. The use of multiple deflations in the numerical solution of singular systems of equations, with applications to potential theory. *SIAM J Numer Anal*, 5:303–322, 1968.

[83] R. MacLeod and D. Brooks. Recent progress in inverse problems in electrocardiology. *IEEE Engineering in Medicine and Biology*, 17:73–83, 1998.

[84] T. Mäkelä, P. Clarysse, O. Sipila, N. Pauna, Q. Pham, T. Katila, and I. Magnin. A review of cardiac image registration methods. *IEEE Trans Med Imaging*, 21:1011–1021, 2002.

[85] T. Mäkelä, Q. Pham, P. Clarysse, J. Nenonen, J. Lötjönen, O. Sipila, H. Hanninen, K. Lauerma, J. Knuuti, T. Katila, and I. Magnin. A 3-d model-based registration approach for the PET, MR and MCG cardiac data fusion. *Med Image Anal*, 7:377–389, 2003.

[86] M. Mäkijärvi, H. Hänninen, P. Korhonen, J. Montonen, and J. Nenonen. Clinical application of magnetocardiographic mapping. In M. Shenasa, M. Borggrefe, and G. Breithardt, eds., *Cardiac Mapping*, pp. 475–486. Blackwell Publishing Inc./Futura Division, 2003.

[87] A. Martinez-Palomo, J. Alanis, and D. Benitez. Transitional cardiac cells of the conductive system of the dog heart. *J Cell Biol*, 47:1–17, 1970.

[88] G. Massing and T. James. Anatomical configuration of the His bundle and bundle branches in the human heart. *Circulation*, 53:609–621, 1976.

[89] C. Mendez, W. Mueller, and X. Urguiaga. Propagation of impulses across the Purkinje fiber-muscle junctions in the dog heart. *Circ Res*, 26:135–150, 1970.

[90] A. MettingVanRijn, A. Kuiper, A. Linnenbank, and C. Grimbergen. Patient isolation in multichannel bioelectic recordings by digital transmission through a single optical fiber. *IEEE Trans Biomed Eng*, 40(3):302–308, 1993.

[91] W. Miller and D. Geselowitz. Simulation studies of the electrocardiogram. I. The normal heart. *Circ Res*, 43:301–314, 1978.

[92] W. Miller and D. Geselowitz. Simulation studies of the electrocardiogram. II. Ischemia and infarction. *Circ Res*, 43:315–323, 1978.

[93] G. Mines. On dynamic equilibrium in the heart. *J Physiol (London)*, 46:349–383, 1913.

[94] T. Montague, E. Smith, D. Cameron, P. Rautaharju, G. Klassen, C. Flemington, and B. Horáček. Isointegral analysis of body surface maps: Surface distribution and temporal variability in normal subjects. *Circulation*, 63:1166–1172, 1981.

[95] J. Nenonen, J. Edens, L. Leon, and B. Horáček. Computer model of propagated excitation in the anisotropic human heart: I. Implementation and algorithms. In K. Ripley and A. Murray, eds., *Computers in Cardiology*. IEEE Computer Society Press, Los Alamitos, CA, 1991.

[96] J. Nenonen, J. Edens, L. Leon, and B. Horáček. Computer model of propagated excitation in the anisotropic human heart: II. Simulation of extracardiac fields. In K. Ripley and A. Murray, eds., *Computers in Cardiology*. IEEE Computer Society Press, Los Alamitos, CA, 1991.

[97] J. Nenonen and B. Horáček. Extracardiac field due to propagated excitation in the ventricular myocardium. In D. Ghista, ed., *Biomedical and Life Physics*, pp. 191–201. Vieweg Verlag, Wiesbaden, 1996.

[98] J. Nenonen, J. Montonen, and R. Koskinen. Surface gradient analysis of atrial activation from magnetocardiographic maps. *International Journal of Bioelectromagnetism*, 5:98–99, 2003.

[99] J. Nenonen, J. Montonen, and M. Mäkijärvi. Principles of magnetocardiographic mapping. In M. Shenasa, M. Borggrefe, and G. Breithardt, eds., *Cardiac Mapping*, pp. 119–129. Blackwell Publishing Inc./Futura Division, 2003.

[100] J. Nenonen, C. Purcell, B. Horáček, G. Stroink, and T. Katila. Magnetocardiographic functional localization using a current dipole in a realistic torso. *IEEE Trans Biomed Eng*, BME-38:658–664, 1991.

[101] T. Oostendorp, A. van Oosterom, and G. Huiskamp. Interpolation on a triangulated 3D surface. *J Comp Physics*, 80:331–343, 1989.

[102] A. v. Oosterom. Modeling the cardiac electric field. *Medical and Biological Engineering and Computing*, 34(Suppl 1):5–8, 1996.

[103] R. Plonsey. *Bioelectric Phenomena*. McGraw-Hill, New York, 1969.

[104] R. Plonsey and R. Barr. Current flow patterns in two-dimensional anisotropic bisyncytia with normal and extreme conductivities. *Biophys J*, 45:557–571, 1984.

[105] A. Pollard and R. Barr. The construction of an anatomically based model of the human ventricular conduction system. *IEEE Trans Biomed Eng*, 37:1173–1185, 1990.

[106] A. Pollard and R. Barr. Computer simulations of activation in an anatomically based model of the human ventricular conduction system. *IEEE Trans Biomed Eng*, 38:982–996, 1991.

[107] M. Potse, A. Linnenbank, H. Peeters, A. SippensGroenewegen, and C. Grimbergen. Continuous localization of cardiac activation sites using a database of multichannel ecg recordings. *IEEE Trans Biomed Eng*, 47:682–689, 2000.

[108] Purkinje. Mikroskopisch-neurologische Beobachtung. *Archiv für Anatomie, Physiologie und wissenschaftliche Medizin*, 1845.

[109] B. Rosenbaum. The hemiblocks: Diagnostic criteria and clinical significance. *Modern Concepts of the Cardiovascular Disease*, 39(12):141–146, 1970.

[110] M. Ross. Muscular tissue. In M. Ross, E. Reith, and L. Romrell, eds., *Histology — A Text and Atlas*, pp. 203–241. Williams & Wilkins, 1989.

[111] B. Roth. Action potential propagation in a thick strand of cardiac muscle. *Circ Res*, 68:162–173, 1991.

[112] B. Roth. A comparison of two boundary conditions used with the bidomain model of cardiac tissue. *Ann Biomedl Eng*, 19:669–678, 1991.

[113] B. Roth. Electrical conductivity values used with the bidomain model of cardiac tissue. *IEEE Trans Biomed Eng*, BME-44:326–328, 1997.

[114] M. Schlüter, M. Geiger, J. Siebels, W. Duckeck, and K. Kuck. Catheter ablation using radiofrequency current to cure symptomatic patients with tachyarrhythmias related to an accessory ventricular pathway. *Circulation*, 84:1644–1661, 1991.

[115] R. Selvester, N. Wagner, and G. Wagner. Ventricular excitation during percutaneous transluminal angioplasty of the left anterior descending coronary artery. *Am J Cardiol*, 62:1116–1121, 1988.

[116] M. Sermesant, Y. Coudiere, H. Delingette, N. Ayache, and J. Desideri. An electromechanical model of the heart for cardiac image analysis. In W. Niessen and M. Viergever, eds., *MICCAI2001, LNCS 2208*, pp. 224–231. Springer-Verlag, Berlin Heidelberg, 2001.

[117] R. M. Shaw and Y. Rudy. Electrophysiologic effects of acute myocardial ischemia: a mechanistic investigation of action potential conduction and conduction failure. *Circ Res*, 80:124–138, 1997.

[118] K. Simelius, T. Jokiniemi, J. Nenonen, I. Tierala, L. Toivonen, and T. Katila. Arrhythmia localization using body surface potential mapping during catheterization. In *Proc 18th Ann Conf IEEE / EMBS*, p. CDROM 975. IEEE Publishing Services, New York, NY, 1996.

[119] K. Simelius, L. Reinhardt, J. Nenonen, I. Tierala, L. Toivonen, and T. Katila. Self-organizing maps in arrhythmia localization from body surface potential mapping. In *Proc 19th Ann Conf IEEE / EMBS*, pp. 62–64. IEEE Publishing Services, New York, NY, 1997.

[120] K. Simelius, I. Tierala, T. Jokiniemi, J. Nenonen, L. Toivonen, and T. Katila. A body surface potential mapping system in clinical use. *Med. & Biol. Eng. & Comput.*, 34(S1):107 –108, 1996.

[121] K. Simelius. *Development of cardiographic mapping techniques for clinical use*. Licenciate thesis, Helsinki University of Technology, 1998.

[122] A. SippensGroenewegen, H. Peeters, E. Jessurun, A. Linnenbank, E. R. de Medina, M. Lesh, and N. van Hemel. Body surface potential mapping during pacing at multiple sites in the human atrium: P-wave morphology of ectopic right atrial activation. *Circulation*, 97:369–380, 1998.

[123] A. SippensGroenewegen, H. Spekhorst, N. van Hemel, J. Kingma, R. Hauer, J. de Bakker, C. Grimbergen, M. Janse, and A. Dunning. Localization of the site of origin of postinfarction ventricular tachycardia by endocardial pace mapping: Body surface mapping compared with the 12-lead electrocardiogram. *Circulation*, 88:2290–306, 1993.

[124] A. SippensGroenewegen, H. Spekhorst, N. van Hemel, J. Kingma, R. Hauer, J. de Bakker, C. Grimbergen, M. Janse, and A. Dunning. Value of body surface mapping in localizing the site of origin of ventricular tachycardia in patients with previous myocardial infarction. *J Am Coll Cardiol*, 24:1708–1724, 1994.

[125] A. SippensGroenewegen, H. Spekhorst, N. van Hemel, J. Kingma, R. Hauer, M. Janse, and A. Dunning. Body surface mapping of ectopic left and right ventricular activation: QRS spectrum in patients without structural heart disease. *Circulation*, 82:879–96, 1990.

[126] A. SippensGroenewegen, H. Spekhorst, N. van Hemel, J. Kingma, R. Hauer, M. Janse, and A. Dunning. Body surface mapping of ectopic left ventricular activation: QRS spectrum in patients with prior myocardial infarction. *Circ Res*, 71:1361–78, 1992.

[127] M. Spach and R. Barr. Ventricular intramural and epicardial potential distributions during ventricular activation and repolarization in the intact heart. *Circ Res*, 37:243–257, 1975.

[128] M. Spach, P. Dolber, J. Heidlage, J. Kootsey, and E. Johnson. Propagating depolarization in anisotropic human and canine cardiac muscle: apparent directional differences in membrane capacitance. a simplified model for selective directional effects of modifying the sodium conductance on v_{max}, τ_{foot}, and the propagation safety factor. *Circ Res*, 60(2):206–219, 1987.

[129] M. Spach, F. Heidlage, E. Darken, E. Hofer, K. Raines, and F. Starmer. Cellular $\dot{V}_{max}$ reflects both membrane properties and the load presented by adjoining cells. *Am J Physiol*, 263:H1855–H1863, 1992.

[130] D. Streeter, Jr. Gross morphology and fiber geometry of the heart. In R. Berne, N. Sperelakis, and S. Geiger, eds., *Handbook of Physiology–Section 2: The Cardiovascular System*, pp. 61–112. Am Physiol Soc, Bethesda, MD, 1979.

[131] B. Taccardi, R. Lux, P. Ershler, R. MacLeod, T. Dustman, and N. Ingebritsen. Anatomical architecture and electrical activity of the heart. *Acta Cardiol*, 52(2):91–105, 1997.

[132] B. Taccardi, E. Macchi, R. Lux, P. Ershler, S. Spaggiari, S. Baruffi, and Y. Vyhmeister. Effect of myocardial fiber direction on epicardial potentials. *Circulation*, 90:3076–3090, 1994.

[133] P. Takala, H. Hänninen, J. Montonen, M. Mäkijärvi, J. Nenonen, L. Oikarinen, K. Simelius, L. Toivonen, and T. Katila. Magnetocardiographic and electrocardiographic exercise mapping in healthy subjects. *Ann Biomed Eng*, 29:501–509, 2001.

[134] S. Tawara. *Das Reizleitungssystem des Säugetierherzens. Eine anatomisch-histologische Studie über das Atrioventrikularbündel und die Purkinjeschen Fädern*. Gustav Fischer Verlag, Jena, 1906.

[135] J. Titus. Normal anatomy of the human cardiac conduction system. *Mayo Clinic Proc*, 48:24–30, 1973.

[136] J. Tranum-Jensen, A. Wilde, J. Vermeulen, and M. Janse. Morphology of electrophysiologically identified junctions between Purkinje fibers and ventricular muscle in rabbit and pig hearts. *Circ Res*, 69:429–437, 1991.

[137] J. Tripp. *Physical Concepts and Mathematical Models*, vol. 66 of *Biomagnetism, An Interdisciplinary Approach*, chap. 6, pp. 101–139. Plenum Press, New York, 1st edn., 1983.

[138] R. Truex. Myocardial cell diameters in primate hearts. *Am J Anat*, 135(2):269–280, 1974.

[139] A. Waller. A demonstration on man of electromotive changes accompanying the heart's beat. *J Physiol (London)*, 8:229–234, 1887.

[140] H. Waxman and M. Josephson. Ventricular activation during ventricular endocardial pacing. I. Electrocardiographic patterns related to the site of pacing. *Am J Cardiol*, 50:1–10, 1982.

[141] H. Wellens, R. Schulenburg, and D. Durrer. Electrical stimulation of the heart in patients with ventricular tachycardia. *Circulation*, 46:216–226, 1972.

[142] F. Wilson. The distribution of the potential differences produced by the heart beat within the body and at its surface. *Am Heart J*, 5:599–616, 1930.

[143] A. Winfree. A spatial scale factor for electrophysiological models of myocardium. *Progress in Biophysics and Molecular Biology*, 69:185–203, 1998.

[144] R. Winslow, D. Scollan, A. Holmes, C. Yung, J. Zhang, and M. Jafri. Elecrophysiological modeling of cardiac ventricular function: From cell to organ. *Annu Rev Biomed Eng*, 2:119–155, 2000.

[145] F. X. Witkowski, K. M. Kavanagh, P. A. Penkoske, and R. Plonsey. In vivo estimation of cardiac transmembrane current. *Circ Res*, 72:424–439, 1993.

[146] Z. Xu, R. Gulrajani, F. Molin, M. Lorange, B. Dubé, P. Savard, and R. Nadeau. A computer heart model incorporating anisotropic propagation. III. Simulation of ectopic beats. *J Electrocardiol*, 29:73–90, 1996.

[147] G.-X. Yan, W. Shimizu, and C. Antzelevitch. Characteristics and distribution of M cells in arterially perfused canine left ventricular wedge preparations. *Circulation*, 98:1921–1927, 1998.

[148] D. Zipes and J. Jalife. *Cardiac electrophysiology — from cell to bedside*. W.B.Saunders, 1995.

ISBN 951-22-7027-7 (Printed version)
ISBN 951-22-7028-5 (Electronic version)
Tampereen Yliopistopaino Oy, Tampere 2004